

2016-01-01

# Design Of A 500 Lbf Liquid Oxygen And Liquid Methane Rocket Engine For Suborbital Flight

Jesus Eduardo Trillo

*University of Texas at El Paso*, [jetrillo@miners.utep.edu](mailto:jetrillo@miners.utep.edu)

Follow this and additional works at: [https://digitalcommons.utep.edu/open\\_etd](https://digitalcommons.utep.edu/open_etd)



Part of the [Aerospace Engineering Commons](#), and the [Mechanical Engineering Commons](#)

---

## Recommended Citation

Trillo, Jesus Eduardo, "Design Of A 500 Lbf Liquid Oxygen And Liquid Methane Rocket Engine For Suborbital Flight" (2016). *Open Access Theses & Dissertations*. 767.

[https://digitalcommons.utep.edu/open\\_etd/767](https://digitalcommons.utep.edu/open_etd/767)

This is brought to you for free and open access by DigitalCommons@UTEP. It has been accepted for inclusion in Open Access Theses & Dissertations by an authorized administrator of DigitalCommons@UTEP. For more information, please contact [lweber@utep.edu](mailto:lweber@utep.edu).

DESIGN OF A 500 LBF LIQUID OXYGEN AND LIQUID METHANE  
ROCKET ENGINE FOR SUBORBITAL FLIGHT

JESUS EDUARDO TRILLO

Master's Program in Mechanical Engineering

APPROVED:

---

Ahsan Choudhuri, Ph.D., Chair

---

Norman Love, Ph.D.

---

Luis Rene Contreras, Ph.D.

---

Charles H. Ambler, Ph.D.  
Dean of the Graduate School

Copyright ©

by

Jesus Eduardo Trillo

2016

DESIGN OF A 500 LBF LIQUID OXYGEN AND LIQUID METHANE  
ROCKET ENGINE FOR SUBORBITAL FLIGHT

by

JESUS EDUARDO TRILLO, B.S.ME

THESIS

Presented to the Faculty of the Graduate School of

The University of Texas at El Paso

in Partial Fulfillment

of the Requirements

for the Degree of

MASTER OF SCIENCE

Department of Mechanical Engineering

THE UNIVERSITY OF TEXAS AT EL PASO

December 2016

## **Acknowledgements**

Foremost, I would like to express my sincere gratitude to my advisor Dr. Ahsan Choudhuri for the continuous support of my Master's study and for giving me the opportunity to conduct research at the UTEP Center for Space Exploration and Technology Research (cSETR) since I was a junior undergraduate student.

Besides my advisor, I would like to thank the rest of my thesis committee, Dr. Norman Love and Dr. Luis Rene Contreras for their encouragement and time to review my thesis.

My sincere thanks to the NASA Johnson Space Center propulsion branch for your guidance, support, and willingness to help my research team on complex rocket engine topics that are invaluable for a successful engine design.

I want to extend my sincere gratitude to all the NASA mentors I had on my five internships. Thank you for giving the opportunity to intern with NASA to gain invaluable experience as an engineer and for helping me grow as a professional and achieve my childhood dream of becoming a NASA engineer.

Another special thanks to all my friends that supported me along the way of this long and sometime hard path and to Mr. Scott Hill for guiding me throughout my research project and striving on helping me become a better engineer each day.

Finally but not least important I want to thank my family and girlfriend for supporting me all the way though my academic and life adventure. To my parents for educating me rightfully into becoming a man of good and the professional I am now. All my achievements are thanks to their support and guidance and I dedicate this degree and my future endeavors to them.

## **Abstract**

Liquid methane (LCH<sub>4</sub>) is the most promising rocket fuel for our journey to Mars and other space entities. Compared to liquid hydrogen, the most common cryogenic fuel used today, methane is denser and can be stored at a more manageable temperature; leading to more affordable tanks and a lighter system. The most important advantage is it can be produced from local sources using in-situ resource utilization (ISRU) technology. This will allow the production of the fuel needed to come back to earth on the surface of Mars, or the space entity being explored, making the overall mission more cost effective by enabling larger usable mass. The major disadvantage methane has over hydrogen is it provides a lower specific impulse, or lower rocket performance.

The UTEP Center for Space Exploration and Technology Research (cSETR) in partnership with the National Aeronautics and Space Administration (NASA) has been the leading research center for the advancement of Liquid Oxygen (LOX) and Liquid Methane (LCH<sub>4</sub>) propulsion technologies. Through this partnership, the CROME engine, a throatable 500 lbf LOX/LCH<sub>4</sub> rocket engine, was designed and developed. The engine will serve as the main propulsion system for Daedalus, a suborbital demonstration vehicle being developed by the cSETR. The purpose of Daedalus mission and the engine is to fire in space under microgravity conditions to demonstrate its restartability. This thesis details the design process, decisions, and characteristics of the engine to serve as a complete design guide.

## Table of Contents

Acknowledgements .....	iv
Abstract .....	v
Table of Contents .....	vi
List of Tables .....	viii
List of Figures .....	ix
Chapter 1: Introduction .....	1
Chapter 2: CROME Purpose and Mission .....	3
Section 2.1: Daedalus Suborbital vehicle overview .....	3
section 2.2: Daedalus mission definition .....	3
Chapter 3: Introduction to Liquid-Propellant Rocket Engines .....	5
Chapter 4: CROME Design Requirements .....	7
Section 4.1: Engine description .....	7
Section 4.2: Engine top level requirements .....	7
4.2.1. Propellants.....	8
4.2.2. Thrust (Ft) and Chamber Pressure (Pc) .....	8
4.2.3. Specific Impulse (Isp) .....	9
4.2.4. Mixture Ratio (MR) .....	10
4.2.5. Nozzle Area Expansion Ratio ( $\epsilon$ ) .....	11
4.2.6. Propellant Feed System.....	14
4.2.7. Type of Engine and Life .....	15
4.2.8. Material .....	15
4.2.9. Chamber Cooling .....	16
4.2.10. Envelope and weight.....	17
Chapter 5: Theoretical Engine Design .....	18
Section 5.1: Thermodynamic properties of propellants .....	18
Section 5.2: Theoretical rocket performance analysis .....	19
5.2.1. Characteristic Velocity (C*) .....	19
5.2.2. Thrust Coefficient (Cf) .....	20

5.2.3. Specific Impulse (Isp) .....	21
5.2.4. Throat Area .....	22
5.2.5. Propellants Flow Rate .....	22
Section 5.3: Thrust chamber geometric parameters .....	23
5.3.1. Combustion Chamber Design .....	23
5.3.2. Nozzle Design .....	26
Chapter 6: Injectors Design .....	32
Section 6.1: Theoretical flow analysis .....	34
Section 6.2: Impinging injector design .....	36
6.2.1. Injector Face .....	37
6.2.2. Injection Orifices Design Guidelines .....	39
6.2.3. Manifolds Design .....	40
Section 6.3: Fixed Pintle injector design .....	43
6.3.1. Design Guidelines .....	45
6.3.2. Manifolds Design .....	47
Section 6.4: Combustion instability analysis .....	50
6.4.1. Introduction to Combustion Instabilities .....	50
6.4.2. High Frequency Instability Analysis .....	52
6.4.3. Acoustic Dampening Devices .....	54
6.4.4. Quarter-wave Resonators Analysis .....	56
Section 6.5: Engine Configuration .....	57
Chapter 7: Conclusion and Future Work .....	60
Bibliography .....	62
Vita .....	64



## **List of Tables**

Table 4.1. Engine operating requirements .....	7
Table 6.1. Transversal modes eigenvalues (Yang & Anderson, 1995) .....	53
Table 6.2. Estimated resonant frequencies for the CROME engine .....	54
Table 6.3. Lengths of quarter-wave resonators for the CROME engine .....	56

## List of Figures

Figure 2.1. Conceptual design of Daedalus spacecraft .....	3
Figure 2.2. Daedalus mission profile .....	4
Figure 3.1. Pressure balance on chamber and nozzle walls (Sutton & Biblarz, 2010).....	6
Figure 4.1. Thrust vs. Chamber Pressure plot for the CROME engine .....	9
Figure 4.2. Specific impulse (Isp) vs. mixture ratio (MR) for LOX/LCH4 propellants .....	11
Figure 4.3. Optimum, under-expanded, and over-expanded nozzles .....	12
Figure 4.4. Isp vs. expansion ratio @ 235 psi chamber pressure.....	13
Figure 4.5. Thrust (vacuum) vs expansion ratio @ 235 psi chamber pressure.....	13
Figure 4.6. Thrust chamber weight increase estimate vs expansion ratio; 0 lbs equals no nozzle	14
Figure 4.7. Material properties of Inconel 625 (Inconel Alloy 625, 2007) .....	16
Figure 5.1. Combustion chamber dimensions.....	24
Figure 5.2. Chamber length relationships used in scaling program (Huzel & Huang, 1992).....	26
Figure 5.3. Conical nozzle contour (Huzel & Huang, 1992) .....	27
Figure 5.4. Bell nozzle contour (Huzel & Huang, 1992).....	27
Figure 5.5. Isp and Thrust (vacuum) vs. expansion ratio @ 235 psi chamber pressure .....	28
Figure 5.6. Thrust efficiency vs. bell nozzle length (Huzel & Huang, 1992).....	29
Figure 5.7. Initial and final parabola angle as a function of expansion ratio (Huzel & Huang, 1992) .....	30
Figure 5.8. CROME thrust chamber final dimensions .....	31
Figure 6.1. Common types of liquid-liquid injector elements (Gill, Nurick, Keller, & Douglass, 1976) .....	33
Figure 6.2. Angular relation of doublet impinging streams (Sutton & Biblarz, 2010).....	37

Figure 6.3. CROME impinging injector face configuration .....	38
Figure 6.4. Impingement resultant angle for CROME impinging injector .....	39
Figure 6.5a. Injector orifice layout at the inlet side .....	41
Figure 6.5b. Isometric view of the closure of the manifolds .....	42
Figure 6.5c. Cross sectional view of impinging injector showing manifold distribution.....	42
Figure 6.6a. Pintle axial/annular flow (Dressler & Bauer, 2000) .....	44
Figure 6.6b. Pintle radial flow (Dressler & Bauer, 2000).....	44
Figure 6.6c. Pintle combined flow- axial and radial (Dressler & Bauer, 2000) .....	44
Figure 6.7. Pintle injector streams angular relation .....	45
Figure 6.8. Key design variables for a pintle injector.....	46
Figure 6.9a. Isometric view of pintle injector.....	48
Figure 6.9b. Pintle injector face configuration .....	48
Figure 6.9c. Cross section view of pintle injector showing manifold distribution .....	49
Figure 6.10a. Isometric view of non-welded version of pintle injector.....	49
Figure 6.10b. Cross section view of non-welded version of pintle injector .....	50
Figure 6.11. High frequency modes of combustion instability (Huzel & Huang, 1992).....	52
Figure 6.12. Chamber wall temperature distribution across thrust chamber .....	53
Figure 6.13. Helmholtz and quarter-wave resonators geometric characteristics .....	55
Figure 6.14. Engine infrastructure – propulsion components.....	58
Figure 6.15. Engine infrastructure – structural supports.....	59

## Chapter 1: Introduction

Liquid methane (LCH<sub>4</sub>) is the most promising rocket fuel for our journey to Mars. Compared to liquid hydrogen, the most common cryogenic fuel used today, methane is denser and can be stored at a more manageable temperature; leading to smaller tanks and a lighter system. The most important advantage is it can be produced from local sources on Mars using in-situ resource utilization (ISRU) technology. This will enable the production of the fuel needed to come back to earth on the Martian surface making the overall mission more affordable. Having this ability also allows for more payload to be carried by the rocket instead of carrying the weight of the fuel. This is particularly important as Mars missions are long and payload capabilities are critical for mission success. Methane has lower specific impulse than Hydrogen, however, the in-situ availability of the fuel will enable much larger payloads.

NASA and several aerospace companies are working on developing their own liquid methane propulsion systems all with the same purpose of enabling the technology to explore Mars and other space entities. Some examples of these engines are the Space X Raptor engine and the Blue Origin BE-4 engine. The NASA Johnson Space Center Morpheus project developed a LOX/LCH<sub>4</sub> engine for use in their lander and Marshall Space Flight Center has tested several LOX/LCH<sub>4</sub> 3D printed rocket engines. The development of liquid methane as rocket fuel is quickly becoming a priority in the space industry and it will be one of the technologies that will make a journey to Mars possible.

The UTEP Center for Space Exploration and Technology Research (cSETR) in partnership with the National Aeronautics and Space Administration (NASA) has been a leading research center for the advancement of Liquid Oxygen (LOX) and Liquid Methane (LCH<sub>4</sub>)

propulsion technologies. Through this partnership, the CROME engine, a throatable 500 lbf LOX/LCH<sub>4</sub> rocket engine, was designed and developed. The engine will serve as the main propulsion system for Daedalus, a suborbital demonstration vehicle being developed by the cSETR. The end purpose of Daedalus mission and the engine is to fire in space under microgravity conditions to demonstrate the performance of an integrated LOX/LCH<sub>4</sub> system in space. There is limited data concerning LOX/LCH<sub>4</sub> rocket engines fired in space and it is of great interest to assess the CROME engine's restartability and throttle capabilities under this condition. The data will serve as a valuable resource to the aerospace community to understand how LOX/LCH<sub>4</sub> propulsion technologies act under microgravity conditions and how they can improve these technologies for future Mars missions.

This thesis describes in detail the complete design process of the engine that includes the engine operating parameters, chamber and nozzle characteristics, injector design, and resonators design. These will include detail description of the assumptions made, formulas used, and the reasoning behind each design decision. This document will serve as a design guide for the cSETR CROME rocket engine.

## Chapter 2: CROME Purpose and Mission

The CROME rocket engine is designed as the main propulsion engine for Daedalus suborbital test vehicle. Most of the engine's operating requirements are derived from this vehicle as well as our understanding of its characteristics and mission.

### SECTION 2.1: DAEDALUS SUBORBITAL VEHICLE OVERVIEW

Daedalus is a suborbital demonstrator vehicle whose mission looks to evaluate performance, restartability, and interaction of the propulsion system under microgravity conditions. The propulsion system consists of a helium pressure regulated propellant feed system that will feed one CROME main engine and 12 cSETR reaction controls engines (RCE) for 3 axis attitude control.

Daedalus is expected to achieve a maximum altitude of 90 miles above sea level and remain in sub-orbit for around 200 seconds. To reach sub orbit, the vehicle will be launched as a payload on top of a Terrier MK12-Improved Orion sounding rocket from NASA Wallops Flight Facility in Virginia, USA. Based on the launch vehicle requirements, Daedalus has to weight no more than 500 lbs and its envelope are limited to 15.75 inches in diameter and 200 inches in length. Figure 2.1 shows the design concept of the Daedalus vehicle.



Figure 2.1. Conceptual design of Daedalus spacecraft

### SECTION 2.2: DAEDALUS MISSION DEFINITION

Daedalus mission flight profile consists of Daedalus being launched from Wallops, Virginia passing the Karman line, or the edge of space, 62 miles above sea level. It will then be

released and the data acquisition and automated control systems will activate to start the vehicle sub orbital maneuvers. The maneuvers consist of an initial attitude adjustment after release and 6 main engine firings at different thrust levels with attitude control as needed. This will serve to demonstrate the main and reaction control engines capability to restart and system operation as a whole under microgravity conditions. After the 6<sup>th</sup> engine firing, the reaction control engines will orient the vehicle to the reentry position to come back to Earth. Figure 2.2 is a representation of the flight profile described.

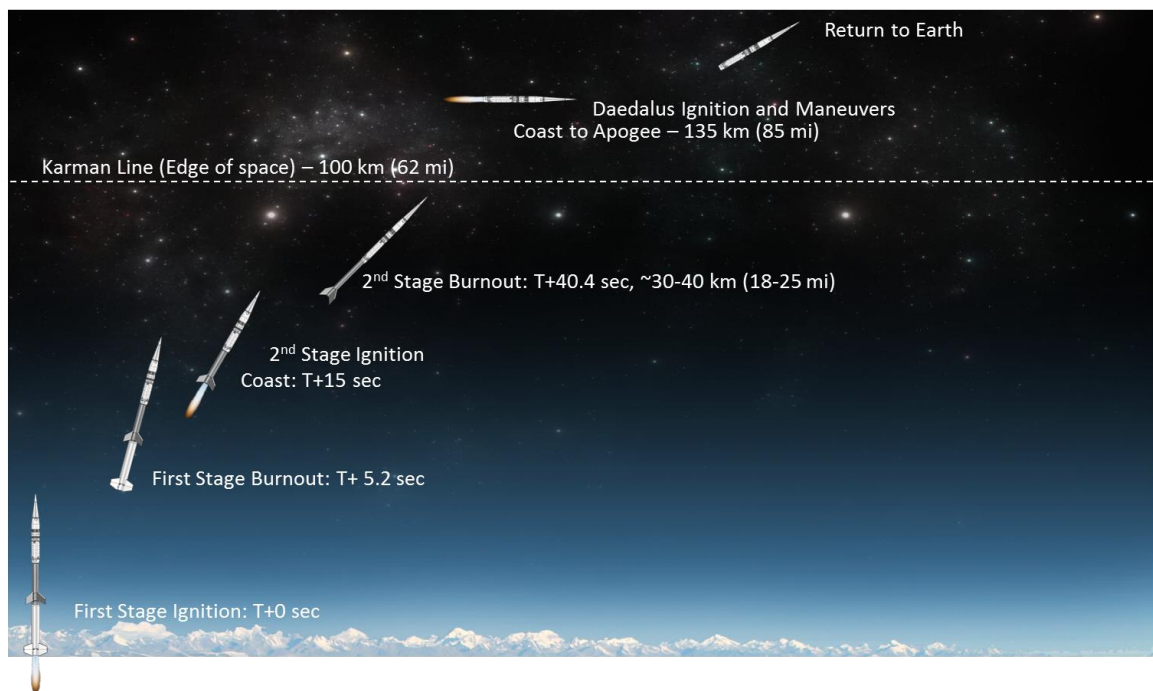


Figure 2.2. Daedalus mission profile

### Chapter 3: Introduction to Liquid-Propellant Rocket Engines

This chapter will briefly explain the basics of how a rocket engine works to set the foundation for the following chapters of this paper.

A bi-propellant rocket engine is conformed of the following basic components:

- 1- Two valves that control the flow of propellants into the engine
- 2- An injector which mixes and atomizes the propellants in the combustion chamber
- 3- A combustion chamber where the propellants combust
- 4- A converging-diverging nozzle where the combustion gases accelerate and expand

The thrust generated by a rocket is the reaction experienced by the structure when ejecting high velocity gases. Thrust can be divided into two terms, momentum and pressure thrust. Momentum thrust is the product of the propellant mass flow rate and the exhaust velocity relative to the vehicle and it accounts for the majority of the thrust generated by a rocket. Pressure thrust is the product of the cross sectional area of the exhaust jet leaving the vehicle and the difference between the exhaust pressure and the surrounding fluid pressure (ambient pressure)<sup>10</sup>. The total thrust of a rocket is defined by equation 3.1 known as the thrust equation:

$$\mathbf{F}_t = \frac{\dot{w}_p}{g_c} \mathbf{V}_e + A_e(\mathbf{P}_e - \mathbf{P}_a) \quad (3.1)$$

The first term is the momentum thrust and the second is the pressure thrust. Notice that if the rocket operates in a vacuum, the ambient pressure ( $P_a$ ) is zero, therefore it generates more thrust in space. On the other hand, if the exit pressure is equal to the ambient pressure ( $P_e = P_a$ ), the whole pressure thrust terms goes away and this is known as optimum expansion.

---

<sup>10</sup>(Huzel & Huang, 1992)



The term specific impulse ( $I_{sp}$ ) is used to measure engine performance. It is defined as the thrust per unit weight flow rate of propellant used,

$$I_{sp} = \frac{F_t}{\dot{w}_p}, (sec) \quad (3.2)$$

Specific impulse is higher in vacuum than at sea level because thrust increases. The units used to describe  $I_{sp}$  is seconds, and is dependent on the thermodynamic properties of the propellants and the quality of the engine design.

Figure 3.1 presents the terms that will be used throughout this paper as well as the pressure balance and velocity relationship on each section of a rocket engine that summarizes the basics of how a rocket engine works.

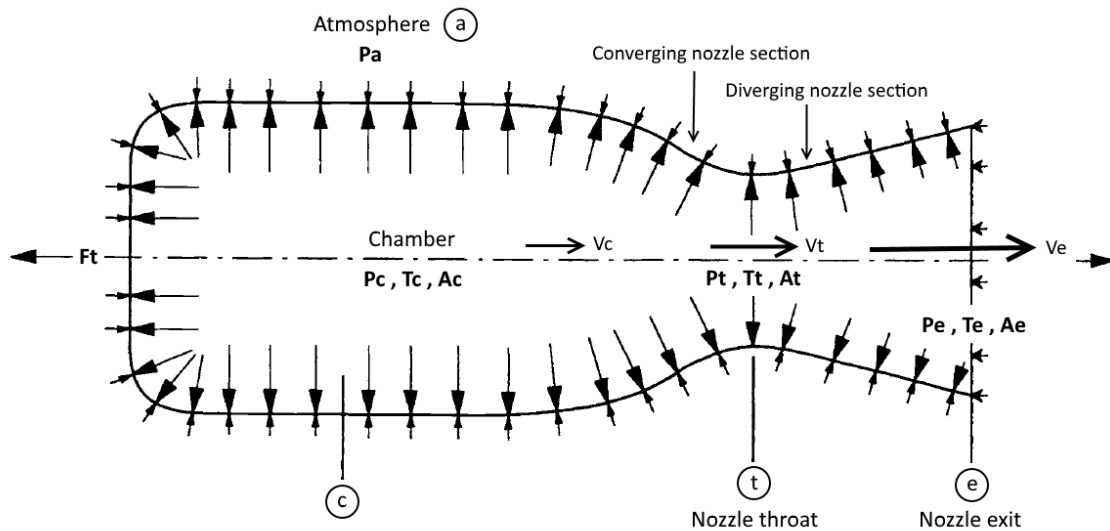


Figure 3.1. Pressure balance on chamber and nozzle walls(Sutton & Biblarz, 2010)

## Chapter 4: CROME Design Requirements

### SECTION 4.1: ENGINE DESCRIPTION

CROME is a rocket engine designed to operate at a sea level thrust of 500 lbf (nominal thrust) and throattable 4:1. It will use Liquid Oxygen (Oxydizer) and Liquid Methane (Fuel) as the propellant combination with a mixture ratio of 2.7 which gives a high specific impulse potential and allows equal volume tanks for the vehicle. Five hundred pounds of thrust is achieved at a nominal chamber pressure of 235 psi with a nozzle having an area expansion ratio of 30:1 for space operation. The engine should be capable of being tested at ambient pressure, therefore, a nozzle extension will be used to go from an area expansion ratio of 1.6:1 (optimum expansion for testing) to the operating area expansion ratio of 30:1 to fit on the given envelope. The engine will be film cooled using liquid methane.

### SECTION 4.2: ENGINE TOP LEVEL REQUIREMENTS

The engine top level design requirements are summarized in table 4.1 below. A brief explanation of each requirement will follow.

Table 4.1. Engine operating requirements

Requirement	Definition / Value
Propellants	Liquid Oxygen (LOX) and Liquid Methane (LCH <sub>4</sub> )
Thrust, (Ft)	500 lbf at sea level; throttable 4:1
Chamber Pressure, (Pc)	70 - 235 psi
Nozzle Area Expansion Ratio ( $\epsilon$ )	1.6 for sea level testing, 30 for space operation
Specific Impulse, (Isp)	227 sec at sea level, 336 sec in vacuum ( $\epsilon = 30$ )
Mixture Ratio (MR)	2.7

<b>Propellant Feed System</b>	Regulated helium pressure fed
<b>Type</b>	Steady state engine
<b>Material</b>	Inconel 625
<b>Chamber Cooling</b>	$\leq 30\%$ fuel film cooling
<b>Envelope</b>	$\leq 14.5$ diameter ; $\leq 24$ " length
<b>Weight</b>	$\leq 70$ lbs

#### 4.2.1. Propellants

The engine will use liquid oxygen (LOX) and liquid methane (LCH<sub>4</sub>) as its propellant combination. The propellant conditions required at injection is saturated liquid at -297 degrees Fahrenheit for liquid oxygen and -259 degrees Fahrenheit for liquid methane.

#### 4.2.2. Thrust (Ft) and Chamber Pressure (Pc)

The engine should be designed to provide a nominal sea level thrust of 500 lbf and have the capability to throttle to a ratio of 4:1, that is, 125 lbf to 500 lbf. The engine is designed at sea level because it is the condition at which it will be tested.

The engine chamber pressure was chosen according to the throttling requirement. The throttling is achieved by increasing or decreasing the pressure drop, or flow rates, by adjusting the percent open of the main valves or changing the injector areas of injection (i.e. pintle injector). In other words, the chamber pressure has to change to have different thrust levels. The critical chamber pressure required for an engine to have sonic, or choked, flow at the throat is around 35 psia at sea level<sup>3</sup>. It was determined that to be on the safe side, we would choose our lowest chamber pressure for our low end thrust (125 lbf) to be 70 psi, double the critical chamber

---

<sup>3</sup>(Brown, 1996)

pressure. To reach our high end thrust, it was determined that 235 psi chamber pressure was required. Figure 4.1 shows the thrust level at different chamber pressure for this engine.

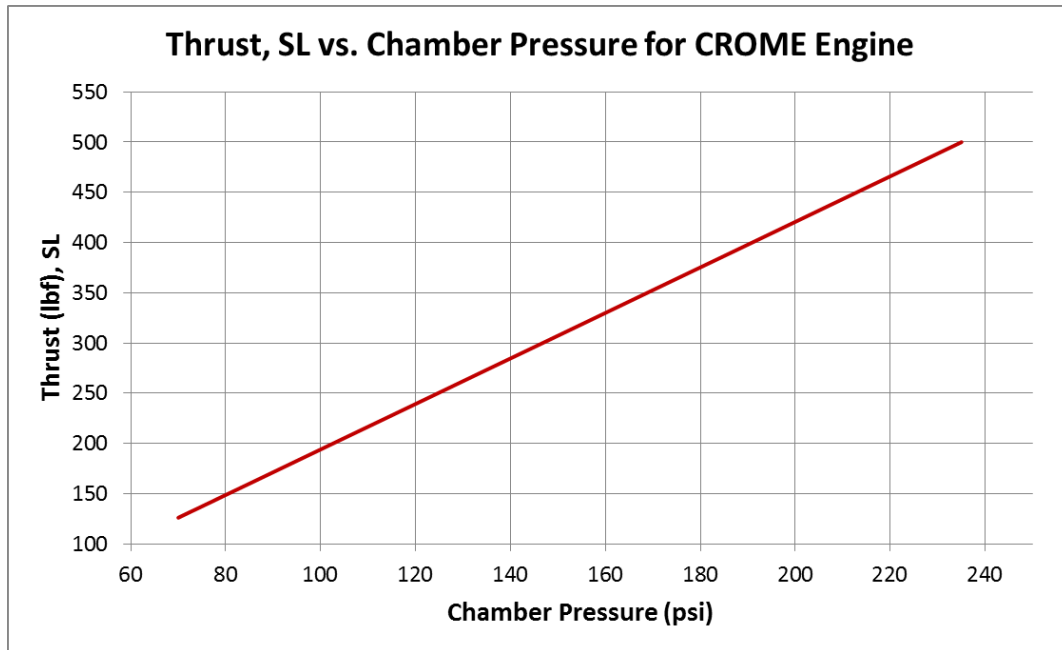


Figure 4.1. Thrust vs. Chamber Pressure plot for the CROME engine

#### 4.2.3. Specific Impulse (Isp)

Specific impulse (Isp) is the premier measurement of rocket performance. It is defined as the thrust per unit weight flow rate of propellant and the maximum achievable Isp relies on the thermodynamic properties of the propellants being used<sup>3</sup>.

$$Isp = \frac{F_t}{\dot{w}_p} \quad (4.1)$$

To determine Isp, a characteristic velocity ( $c^*$ ) efficiency of 95%, a thrust coefficient ( $C_f$ ) efficiency of 96%, and an addition of 30% of the fuel flow for cooling was assumed. These

percentages were chosen according to what our mentors at NASA JSC used for their Morpheus engine design. Note that the addition of fuel for cooling will decrease the Isp as more propellant flow is being used. The Isp at sea level was estimated to be a nominal 227 seconds and 336 seconds in vacuum. The full details of the assumptions and calculations for Isp are described in chapter 5.

#### 4.2.4. Mixture Ratio (MR)

The mixture ratio is defined as the ratio of the oxidizer to fuel mass flow rate,

$$MR = \frac{\dot{m}_o}{\dot{m}_f} \quad (4.2)$$

An analysis was performed using Rocket Propulsion Analysis (RPA) software written by Alexander Ponomarenko. RPA uses NASA's Chemical Equilibrium with Applications (CEA) library to determine the thermodynamic properties of different propellants to perform rocket engine analysis<sup>13</sup>. The analysis performed was conducted to determine the optimum mixture ratio for the system. Using a chamber pressure of 235 psi and our two propellants, a plot of mixture ratio against specific impulse (Isp) was obtained and shown in figure 4.2.

---

<sup>13</sup>(Ponomarenko, 2015)

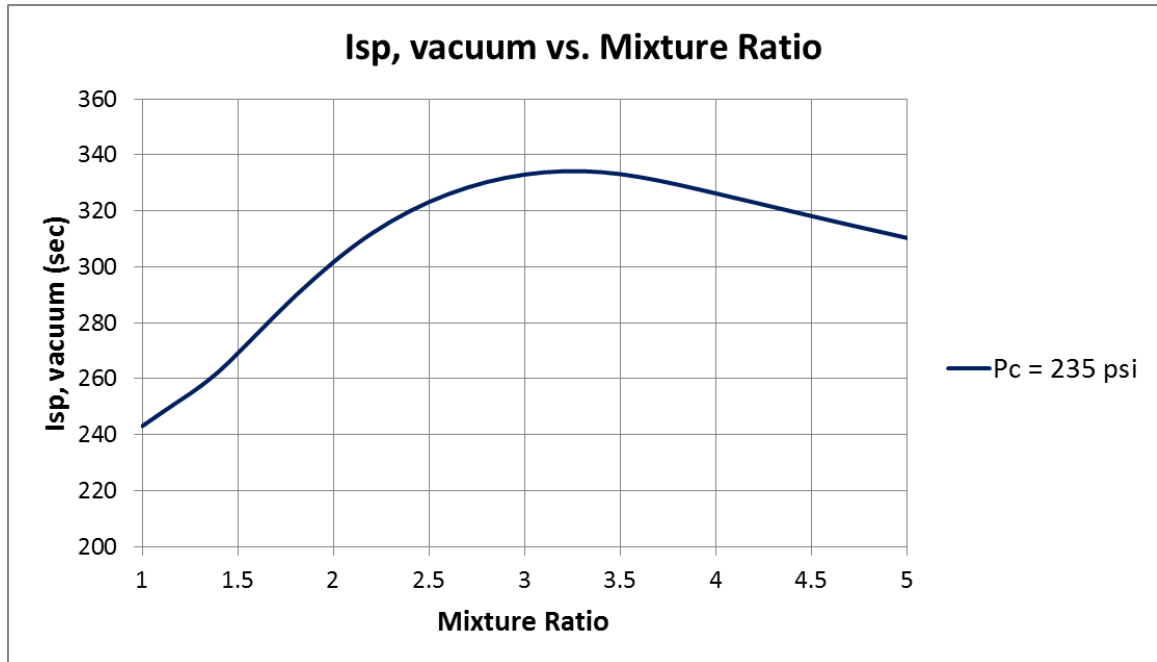


Figure 4.2. Specific impulse (Isp) vs. mixture ratio (MR) for LOX/LCH4 propellants

The highest specific impulse (Isp) is obtained at around 3.2 mixture ratio. The MR was chosen to be 2.7 as it offers a high Isp potential and it allows equal volume propellant tanks for Daedalus vehicle.

#### 4.2.5. Nozzle Area Expansion Ratio ( $\epsilon$ )

A rocket engine takes advantage of the supersonic velocity increase that can be achieved in a converging-diverging nozzle (de Laval nozzle). The nozzle expansion ratio is the ratio between the exit area of the nozzle to the area of the throat<sup>3</sup>:

$$\epsilon = \frac{A_e}{A_t} \quad (4.3)$$

For testing conditions, an area expansion ratio of 1.6 was calculated using equation 4.4:

---

<sup>3</sup>(Brown, 1996)

$$\frac{A_e}{A_t} = \frac{\sqrt{k \left( \frac{2}{k+1} \right)^{\frac{k+1}{k-1}}}}{\left( \frac{P_e}{P_c} \right)^{\frac{1}{k}} \sqrt{\frac{2k}{k-1} \left[ 1 - \left( \frac{P_e}{P_c} \right)^{\frac{k-1}{k}} \right]}} \quad (4.4)$$

To get the optimum expansion at El Paso, TX ambient conditions ( $P_a=12.7$  psi), we equal  $P_e=P_a$ . It is desired to have optimal expansion when testing, but because the engine will throttle, an under-expanded nozzle across the thrust range is preferable. To achieve this, the nozzle expansion ratio for testing needs to be optimum at the lowest chamber pressure ( $P_c=70$  psi). An under-expanded nozzle will affect the performance of the engine but it is more desirable than having an over-expanded nozzle as the flow will begin to separate inside the divergent portion affecting performance and thrust more significantly<sup>14</sup>. The specific heat ratio ( $k$ ) for our propellants is obtained using NASA CEA software as described in chapter 5 section 5.1 of this paper.

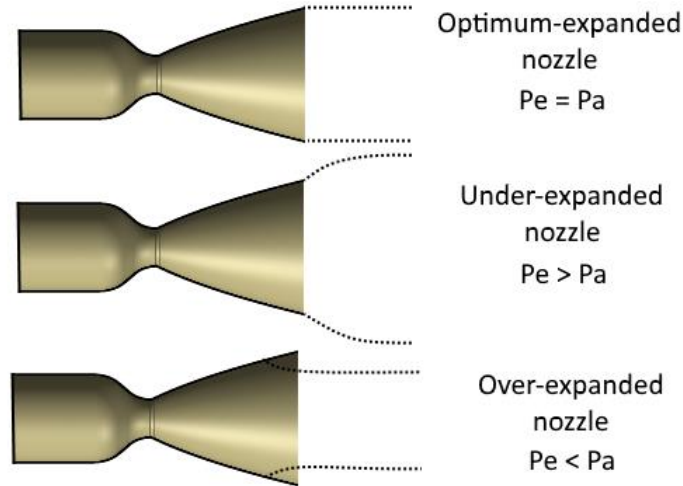


Figure 4.3. Optimum, under-expanded, and over-expanded nozzles

<sup>14</sup>(Sutton & Biblarz, 2010)

For vacuum operation, the optimum area expansion ratio is infinity as the nozzle exit pressure gets closer to zero as we increase expansion ratio. The decision to select the space operation expansion ratio was constraint by the weight and dimension limits set by the vehicle and driven by the thrust and performance increase. The plots shown below represent an analysis done to help select the space expansion ratio comparing it with Isp, thrust and weight.

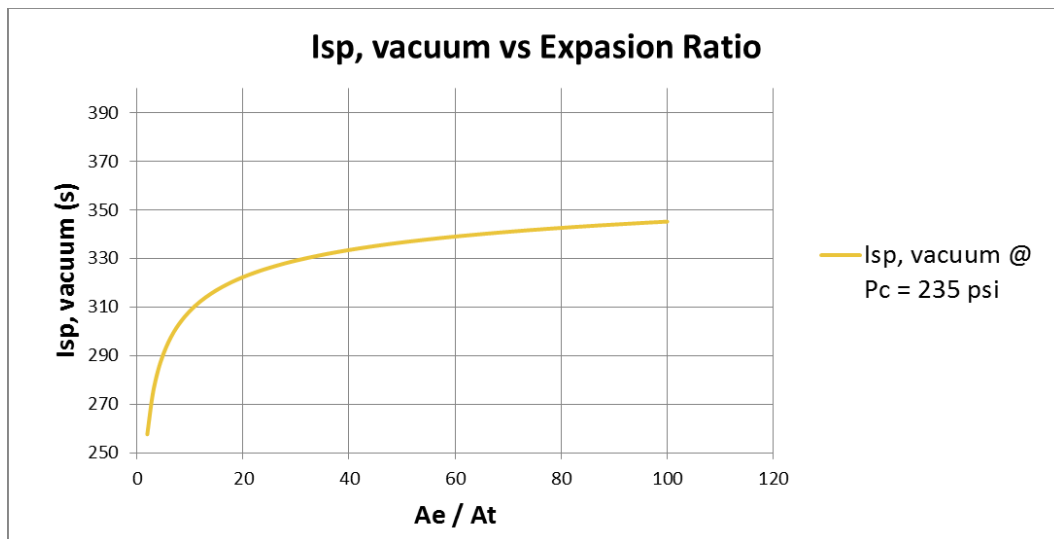


Figure 4.4. Isp vs. expansion ratio @ 235 psi chamber pressure

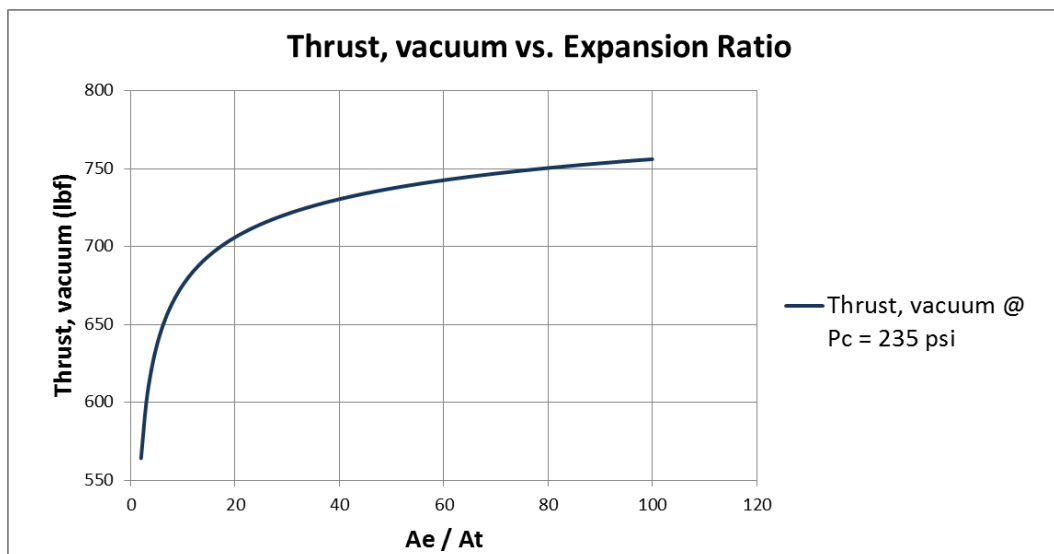


Figure 4.5. Thrust (vacuum) vs expansion ratio @ 235 psi chamber pressure



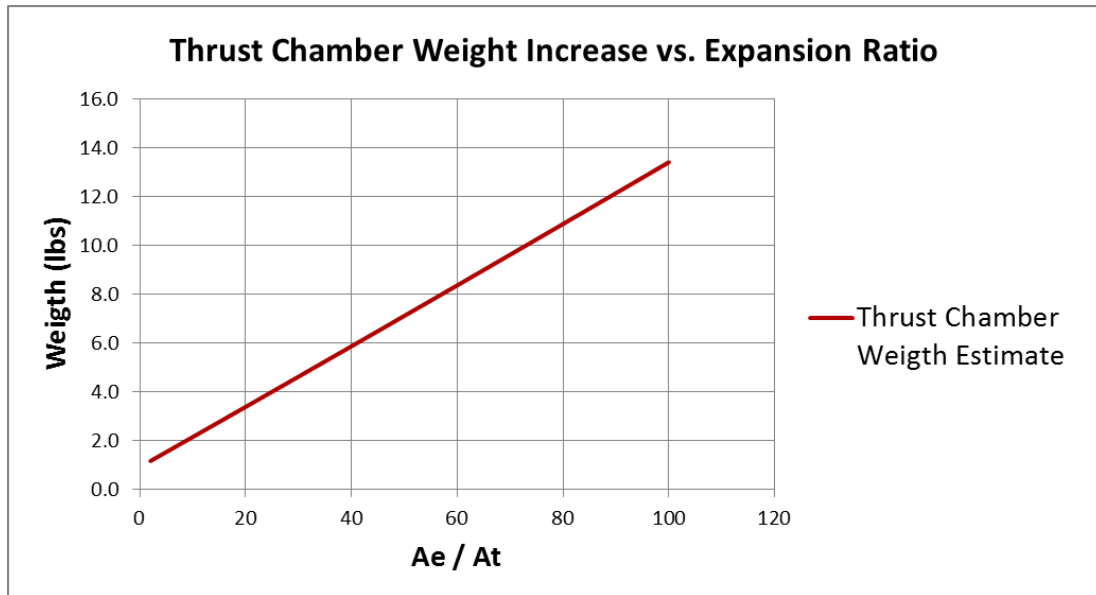


Figure 4.6. Thrust chamber weight increase estimate vs expansion ratio; 0 lbs equals no nozzle

According to these plots, at an expansion ratio of approximately 60 the thrust and Isp plots start to asymptote, but because of the envelope constraints of the vehicle, an expansion ratio of 30 was selected for space operation. This expansion ratio will still give us a significant boost in thrust and Isp and the weight will be maintained to a minimum.

#### 4.2.6. Propellant Feed System

One of the simplest and most common ways of delivering the propellant is by pressurizing the tanks with high pressure gas. The system chosen for Daedalus and the engine is a Helium gas pressure regulated system. This type of system has the advantage of delivering constant pressure which delivers constant propellant flow and approximately constant thrust, Isp, and mixture ratio<sup>14</sup>. This is important as the engine will be fired several times at several thrust

<sup>14</sup>(Sutton & Biblarz, 2010)

levels during its mission and constant pressure output is important to be able to better control the throttability of the engine.

#### **4.2.7. Type of Engine and Life**

The engine is defined to be a steady state engine. It has to burn for 200 seconds total with 6 engine restarts according to the vehicle mission requirements, but its life will not be limited by this. The thrust chamber will be designed to have infinite life assuming appropriate cooling.

#### **4.2.8. Material**

The material chosen for the thrust chamber and injectors is Inconel 625. This high temperature steel alloy is commonly used for aerospace applications because of its relatively high melting temperature of 2300 – 2437 °F, good strength properties at elevated temperatures, and short lead time<sup>1</sup>. Compared to other high temperature materials used in rocket engines (i.e. Monel and Columbium), Inconel has a lower melting temperature, which means a significant loss in Isp due to the increase of fuel needed for cooling, but it costs a fraction and is readily available. Also, Inconel 625 can be 3D printed and one of the goals of this engine is to explore the possibility of using additive manufactured components. Figure 4.6 shows the material properties of Inconel 625.

---

<sup>1</sup>(Inconel Alloy 625, 2007)

Density, lb/cu in.....	0.305
gram/cc.....	8.44
Melting Range, °F.....	2350-2460
°C.....	1290-1350
Specific Heat <sup>a</sup> , Btu/lb°F (J/kg°C)	
0°F (-18°C).....	0.096 (402)
70°F (21°).....	0.098 (410)
200°F (93°C).....	0.102 (427)
400°F (204°C).....	0.109 (456)
600°F (316°C).....	0.115 (481)
800°F (427°C).....	0.122 (511)
1000°F (538°C).....	0.128 (536)
1200°F (649°C).....	0.135 (565)
1400°F (760°C).....	0.141 (590)
1600°F (871°C).....	0.148 (620)
1800°F (982°C).....	0.154 (645)
2000°F (1093°C).....	0.160 (670)
Permeability at 200 Oersted (15.9 kA/m).....	1.0006
Curie Temperature, °F.....	<-320
°C.....	-196

<sup>a</sup>Calculated

Temp. °F	Modulus of Elasticity, 10 <sup>3</sup> ksi				Poisson's Ratio	
	Tension		Shear		Annealed	Solution-Treated
	Annealed	Solution-Treated	Annealed	Solution-Treated		
70	30.1	29.7	11.8	11.3	0.278	0.312
200	29.6	29.1	11.6	11.1	0.280	0.311
400	28.7	28.1	11.1	10.8	0.286	0.303
600	27.8	27.2	10.8	10.4	0.290	0.300
800	26.9	26.2	10.4	10.0	0.295	0.302
1000	25.9	25.1	9.9	9.6	0.305	0.312
1200	24.7	24.0	9.4	9.2	0.321	0.314
1400	23.3	22.8	8.7	8.8	0.340	0.305
1600	21.4	21.5	8.0	8.3	0.336	0.289

Figure 4.7. Material properties of Inconel 625 (Inconel Alloy 625, 2007)

#### 4.2.9. Chamber Cooling

Due to the high temperature (5800 °F) of the combustion process in the engine, a cooling method for the chamber wall needs to be implemented to avoid engine failure. The method

selected was fuel film cooling (FCC) in addition to radiation cooling. Fuel film cooling works by introducing a thin film of fuel into the combustion chamber wall through orifices found on the periphery of the injector plate. This film is a thermal barrier between the combustion gases and the combustion chamber. This is one of the easiest cooling methods to implement but it will degrade engine performance. The NASA Johnson Space Center Morpheus project used film cooling for their Morpheus LOX/LCH<sub>4</sub> engine. They tested their engine and determined that 30% film cooling (30% of the fuel flow rate for combustion) was enough to maintain the engine properly cooled. According to this, it was decided to design to a maximum of 30% FCC. The injector will be designed with the capability to adjust the amount of coolant introduced to find the lowest percentage needed that will efficiently cool the engine.

#### **4.2.10. Envelope and weight**

The maximum envelope and weight limits for the engine are defined by the Daedalus vehicle. The engine package, which consists of thrust chamber (combustion chamber and nozzle), injector, valves, igniter, and any plumbing and fittings needed to interface in between, has to fit inside an envelope of 14.5” in diameter and 24” in length and weight less than 70 lbs.

## Chapter 5: Theoretical Engine Design

### SECTION 5.1: THERMODYNAMIC PROPERTIES OF PROPELLANTS

If the flow on a rocket engine is idealized, thermodynamics can be used to predict rocket performance. Certain correction factors will be used for better analysis. The following assumptions are made for ideal gas flow calculations for rocket thrust chambers<sup>39 1014</sup>:

- 1- Homogeneous gas composition
- 2- Combustion gases follow the perfect gas laws because the temperature is above vapor conditions
- 3- No heat transfer through the nozzle wall
- 4- No friction therefore there is no boundary layer
- 5- One dimensional flow; all the gases leave the engine axially
- 6- Gas velocity is uniform across any section normal to the nozzle axis
- 7- Steady and constant flow rate
- 8- Chemical equilibrium is established in the combustion chamber and remains throughout the nozzle

Assumptions 3 to 6 permits the use of one-dimensional isentropic expansion relations. To obtain the thermodynamic properties of liquid oxygen (LOX) and liquid methane (LCH<sub>4</sub>) propellant combination, NASA Chemical Equilibrium with Applications (CEA) software is used. The inputs required are:

- a. Propellants : LOX and LCH<sub>4</sub>

---

<sup>3</sup>(Brown, 1996)

<sup>9</sup>(Hill & Peterson, 1965)

<sup>10</sup>(Huzel & Huang, 1992)

<sup>14</sup>(Sutton & Biblarz, 2010)

- b. Chamber Pressure ( $P_c$ ) range : 70 to 235 psi
- c. Mixture Ratio (MR) : 2.7
- d. Expansion Ratio or Supersonic Area Ratio ( $\epsilon$ ) : 1.6 for ambient testing and 30 for space operation

Note that CEA calculates the thermodynamic properties of our propellant combination at each chamber pressure defined by the minimum, maximum, and interval values that one inputs. The following output values are for the combustion products of liquid oxygen and liquid methane and are used for the rocket performance analysis:

- Specific heat ratio ( $k$ ): 1.35
- Specific gas constant ( $R$ ): 0.10 Btu/ lbmol R
- Molecular weight (MW): 19 lb/lbmol
- Chamber temperature ( $T_c$ ): 5545 - 5750 R
- Nozzle exit pressure ( $P_e$ ) for: 12 – 42 psi ( $\epsilon = 1.6$ ) and 0.19 – 0.52 psi ( $\epsilon = 30$ )

Note: the chamber temperature and nozzle exit pressure values are for min and max chamber pressure accordingly (i.e. 5545 R chamber temperature is for 70 psi chamber pressure and 5750 R is for 235 psi).

## **SECTION 5.2: THEORETICAL ROCKET PERFORMANCE ANALYSIS**

This section will be divided in subsections in the order of how things were calculated to make the analysis easier to follow.

### **5.2.1. Characteristic Velocity ( $C^*$ )**

Characteristic velocity (pronounced “cee-star”) is an empirical rocket parameter used to separate the thermochemical performance of propellants from the performance of a particular

engine design. It measures combustion performance by indicating how many pounds of propellant must be burned to maintain the required chamber pressure. It is independent of nozzle performance and is not affected by ambient pressure<sup>3</sup>. Characteristic velocity is defined by the following expression:

$$c^* = \frac{P_c A_t g_c}{\dot{w}_p} = \frac{\sqrt{k g_c R T_c}}{k \sqrt{\left(\frac{2}{k+1}\right)^{\frac{k+1}{k-1}}}}, (ft/sec) \quad (5.1)$$

As one can see by the second expression, characteristic velocity is a function of the propellant properties (combustion gases) in the combustion chamber. Typical correction factors for the characteristic velocity, based on previous engine development programs, range from 0.87 to 1.03<sup>10</sup>. The correction factor used is 0.95 as it is what is typically achieved during steady state performance<sup>3</sup>. The C\* range calculated for our minimum and maximum chamber pressure accordingly is 5716 –5769 ft/s.

### 5.2.2. Thrust Coefficient (Cf)

The thrust coefficient represents the improvement of thrust provided by the gas expansion through the nozzle, as compared to the force which will be generated by the chamber pressure acting only on the throat<sup>10</sup>. In other words, an engine without a diverging section would have a thrust coefficient of 1.0<sup>3</sup>. Thrust coefficient is defined as:

---

<sup>3</sup>(Brown, 1996)

<sup>10</sup>(Huzel & Huang, 1992)

<sup>3</sup>(Brown, 1996)

$$C_f = \frac{F_t}{A_t P_c} = \sqrt{\frac{2 k^2}{k-1} \left(\frac{2}{k+1}\right)^{\frac{k+1}{k-1}} \left[1 - \left(\frac{P_e}{P_c}\right)^{\frac{k-1}{k}}\right]} + \left(\frac{P_e - P_a}{P_c}\right) \frac{A_e}{A_t} \quad (5.2)$$

The typical correction factor for thrust coefficient, based on past engine development programs, is between 0.92 – 1.00<sup>10</sup>. The value used is 96% as it is a value in between the range. The  $C_f$  calculated for our engine is 1.1 – 1.3 for the min and max chamber pressure accordingly at ambient pressure. A  $C_f$  of 1.88 was calculated for vacuum conditions.

### 5.2.3. Specific Impulse (Isp)

The specific impulse (Isp) is defined as the total thrust produced per unit weight of propellant flow. It is the premier measurement of rocket performance similar to the miles per gallon measurement is for cars. Isp is dependent on the propellant combination and the quality of the engine design. That is why Isp is used to compare different propellant combinations and the efficiency of rocket engines. Specific impulse is defined by the following expression<sup>3</sup>:

$$Isp = \frac{F_t}{\dot{w}_p} = \frac{C_f C^*}{g_c} = \sqrt{\frac{2 k R T_c}{g_c (k-1)} \left[1 - \left(\frac{P_e}{P_c}\right)^{\frac{k-1}{k}}\right]}, (sec) \quad (5.3)$$

In the formula above, notice the last expression for Isp. At sea level, higher chamber pressures will give higher Isp. If the engine operates in a vacuum, the  $\left[1 - \left(\frac{P_e}{P_c}\right)^{\frac{k-1}{k}}\right]$  term goes away as the exit pressure approaches zero for a space engine, therefore chamber pressure does not affect specific impulse in space. This is why space engines usually are designed to have low chamber pressures<sup>3</sup>.

---

<sup>3</sup>(Brown, 1996)



To calculate the theoretical Isp delivered by the engine, the second expression using the characteristic velocity ( $C^*$ ) and the thrust coefficient ( $C_f$ ) is used. Note that the  $C^*$  and  $C_f$  value calculated already have a correction factor included. The theoretical sea level Isp for this engine is 227 seconds and 336 seconds in vacuum, both at maximum chamber pressure. The sea level Isp at the low chamber pressure is 190 seconds.

#### 5.2.4. Throat Area

To calculate the area of the throat, the thrust coefficient expression is used:

$$C_f = \frac{F_t}{A_t P_c} \rightarrow A_t = \frac{F_t}{P_c C_f}, (in^2) \quad (5.4)$$

The max chamber pressure ( $P_c=235$  psi) will be used for this calculation as well as its corresponding thrust coefficient ( $C_f = 1.3$ ) and thrust ( $F_t = 500$  lbf) values. The throat area is  $1.68 in^2$  which corresponds to a throat diameter of 1.46 in. If the low end thrust is calculated using 70 psi as chamber pressure, its corresponding  $C_f$ , and the calculated throat area, the value comes up to the desired 125 lbf.

#### 5.2.5. Propellants Flow Rate

To determine the total required propellant flow rate to obtain the desired thrust, the following formula is used:

$$\dot{w}_p = \frac{F_t}{I_{sp}}, (lb/sec) \quad (5.5)$$

The total propellant flow rate required to get our required thrust range, 125 – 500 lbf, is 0.66 – 2.2 lb/sec accordingly. To calculate the individual propellant flow rates, including the film cooling, we will use the selected mixture ratio ( $MR = 2.7$ ) and the film cooling percentage (30%) as follows:

$$\dot{w}_{fuel} = \frac{\dot{w}_p}{MR+1} \quad (5.6)$$

$$\dot{w}_{ox} = \dot{w}_p - \dot{w}_{fuel} \quad (5.7)$$

$$\dot{w}_{fc} = 0.3 \dot{w}_{fuel} \quad (5.8)$$

The corresponding values for the thrust range are 0.48 – 1.6 lb/sec for LOX, 0.18 – 0.59 lb/sec for LCH<sub>4</sub>, and 0.05 – 0.18 lb/sec for fuel film cooling.

## SECTION 5.3: THRUST CHAMBER GEOMETRIC PARAMETERS

### 5.3.1. Combustion Chamber Design

The combustion chamber is the part of the rocket engine where the combustion of propellants takes place. Proper atomization, mixing and combustion of propellants is important for engine performance and is a function of many parameters such as propellant combination, injected conditions of propellants (liquid, gas), combustor geometry, and injector design<sup>10</sup>. The theoretical required combustion chamber volume is a function of the mass flow rate of propellants, the average density of combustion products, and the stay time needed for efficient combustion. The term “stay time” is the average value of the time spent by each propellant gas molecule within the chamber volume. This parameter is very hard to predict and has to be determined experimentally.

A term that is more useful in determining the combustion chamber volume is the characteristic chamber length ( $L^*$ ) pronounced “el star”, and is defined by the following expressions:

---

<sup>10</sup>(Huzel & Huang, 1992)

$$L^* = \frac{V_c}{A_t}, (in) \quad (5.9)$$

$$V_c = A_c L_{cyl} + A_c L_{cone} \left( 1 + \sqrt{\frac{A_t}{A_c}} + \frac{A_t}{A_c} \right), (in^3) \quad (5.10)$$

In the expressions described above,  $V_c$  is the approximate chamber volume, “ $A_t$ ” is the area of the throat,  $L_{cyl}$  is the cylindrical length,  $L_{cone}$  ( $L_c - L_{cyl}$ ) is the length of the converging nozzle section, and  $A_t/A_c$  is the reciprocal of the chamber contraction ratio ( $\epsilon_c = A_c/A_t$ )<sup>14</sup>.

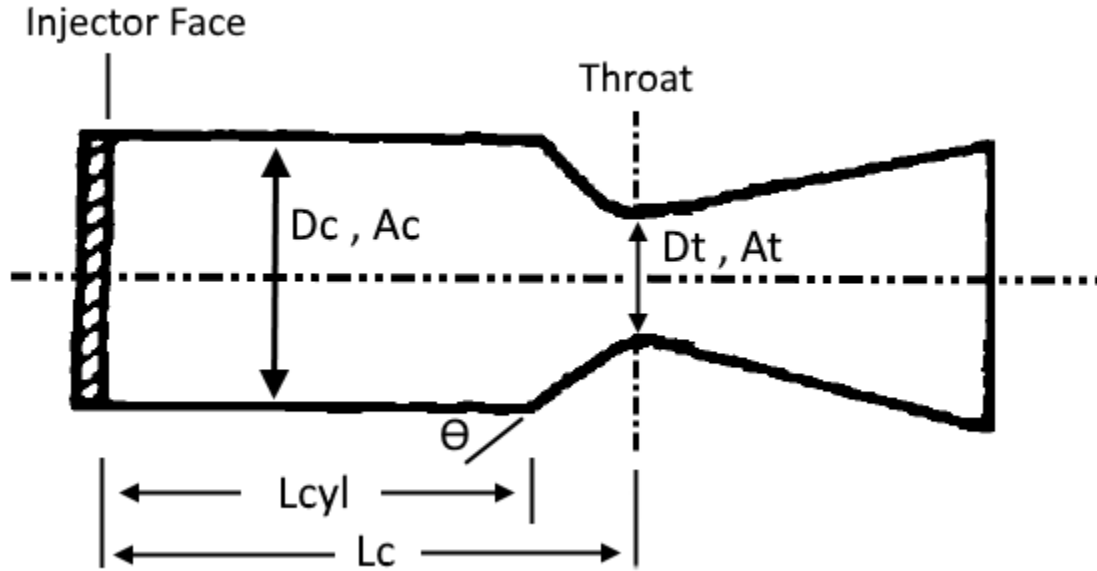


Figure 5.1. Combustion chamber dimensions

The use of  $L^*$  for combustion chamber design is useful because it is a parameter that can be varied and experimentally tested for engine performance optimization or it can be chosen using data from successful engines of similar designs and identical propellants. A larger  $L^*$  means more volume for complete atomization, mixing and, combustion, but it will result in higher thrust chamber volume and weight, surface area increase resulting in more coolant needed to

<sup>14</sup>(Sutton & Biblarz, 2010)

cool the chamber wall and an increase of frictional losses reducing nozzle stagnation pressure resulting in loss of thrust<sup>10</sup>.

In the case of the CROME engine, we have the guidance and mentorship of NASA JSC Morpheus project engineers and according to their engine design and testing, they recommended an  $L^*$  value between 20 and 30 inches for our application.

Our combustion chamber will be a cylindrical chamber, instead of spherical or near spherical shape, because is easier to manufacture and is the most used in US industry. To determine the chamber volume, first the chamber diameter and cross sectional area has to be determined. The main factor constraining our chamber diameter is the space needed for our injector design and acoustic cavities. After several iterations between chamber diameter and injector design, the smallest diameter needed was 3.5 inches, which gives a chamber cross sectional area of 9.7 in<sup>2</sup> and a contraction ratio of 5.8.

An  $L^*$  value of 22 in was chosen to be just above the minimum recommended to have a smaller chamber volume, which equates approximately to 36 in<sup>3</sup> using equation 5.9. It is important to keep a small chamber volume to minimize the surface area that requires cooling and the length that the film cooling stream needs to travel to reach the throat.

A total chamber length ( $L_c$ ) of 4.75 inches was chosen using the graph in figure 5.2 as a baseline knowing the throat diameter of the engine ( $D_t = 1.46$  in). Theta ( $\Theta$ ) was chosen arbitrarily to be 45° as it is not a critical design parameter as it will not affect performance<sup>14</sup>. The cylindrical length ( $L_{cyl}$ ) and the converging nozzle length ( $L_{cone}$ ) are derived to be 2.77 inches and 1.98 inches accordingly using equation 5.10.

---

<sup>14</sup>(Sutton & Biblarz, 2010)

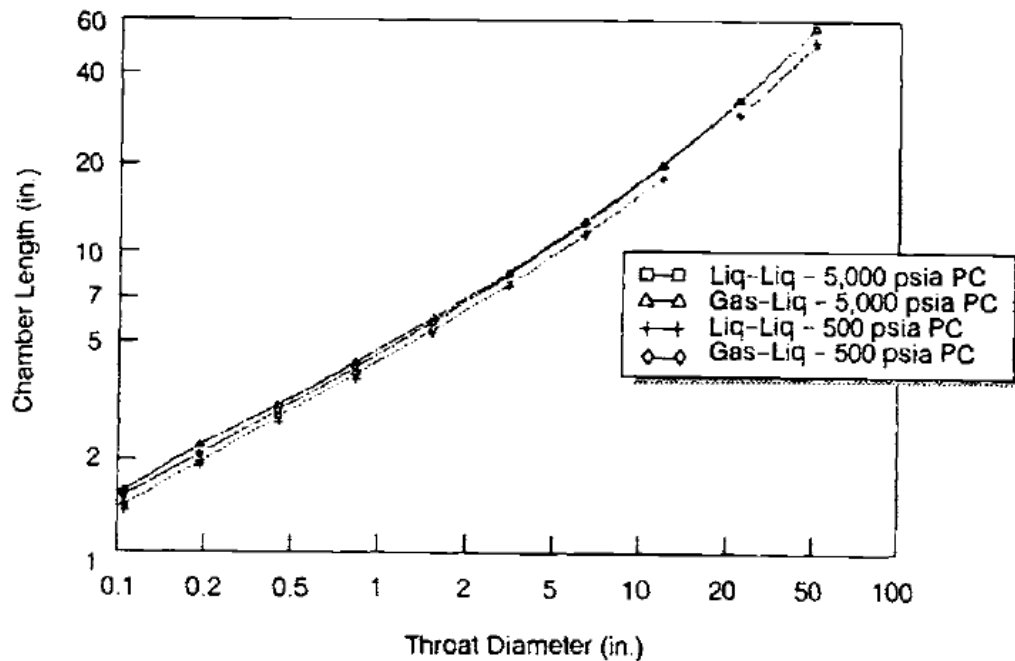


Figure 5.2. Chamber length relationships used in scaling program (Huzel & Huang, 1992)

### 5.3.2. Nozzle Design

The converging-diverging nozzle is the part of the engine where the combustion thermal energy is converted into kinetic energy. The pressure and temperature drop dramatically and the gas velocity reaches supersonic velocity. It is a reversible, essentially isentropic flow process. The objectives of a good nozzle configuration are to obtain the highest practical  $I_{sp}$ , minimize inert nozzle mass, and conserve length to minimize vehicle length, vehicle structure, and vehicle inert mass<sup>14</sup>.

There are different types of nozzles, but the most widely used are conical and bell shaped nozzles. Conical nozzles are most commonly used in small thrusters. They are the easiest to manufacture and allows for easy design change to higher or lower area expansion ratios without major redesign<sup>14</sup>.

<sup>14</sup>(Sutton & Biblarz, 2010)

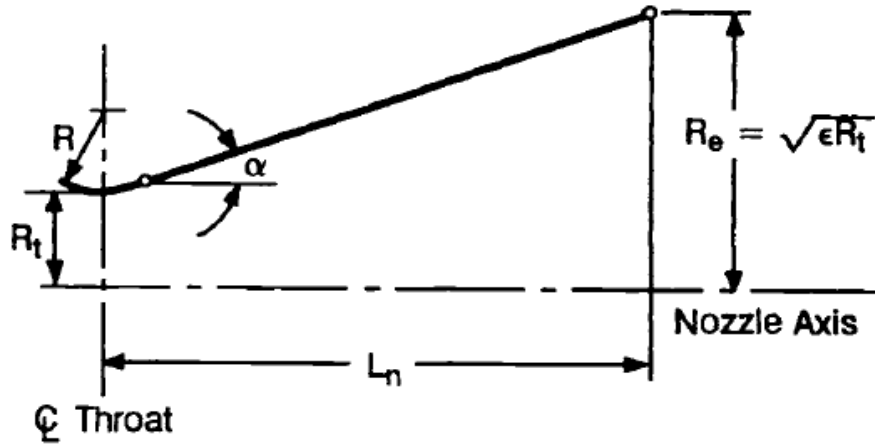


Figure 5.3. Conical nozzle contour (Huzel & Huang, 1992)

Bell nozzles are the most commonly used nozzles as they are designed to gain higher performance having a shorter length. It employs a fast expansion (radial flow) section in the initial divergent section, which lead to a uniform, axially directed flow at the nozzle exit. The contour is changed gradually (parabola shaped) to prevent oblique shocks that affect performance<sup>10</sup>.

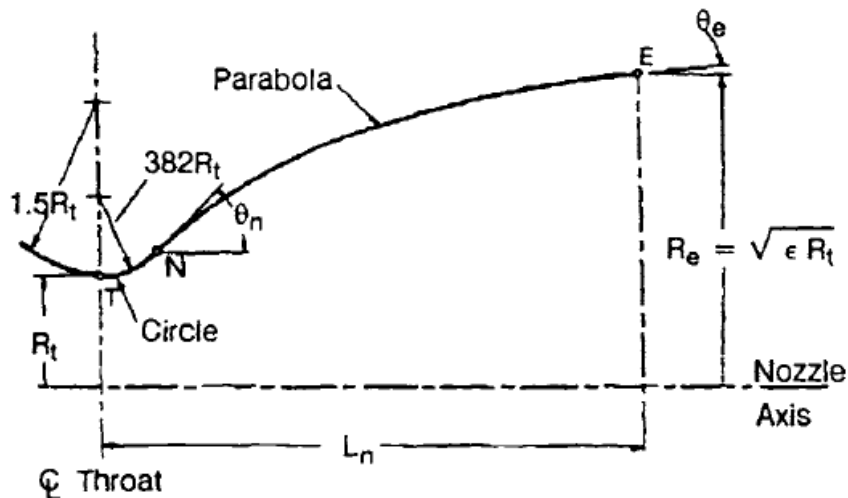


Figure 5.4. Bell nozzle contour (Huzel & Huang, 1992)

<sup>10</sup>(Huzel & Huang, 1992)

A bell nozzle was chosen for the engine because it will reduce length and inert mass. To choose the space expansion ratio, an analysis between area expansion ratio against Isp and thrust was performed using RPA and plotted in figure 5.5.

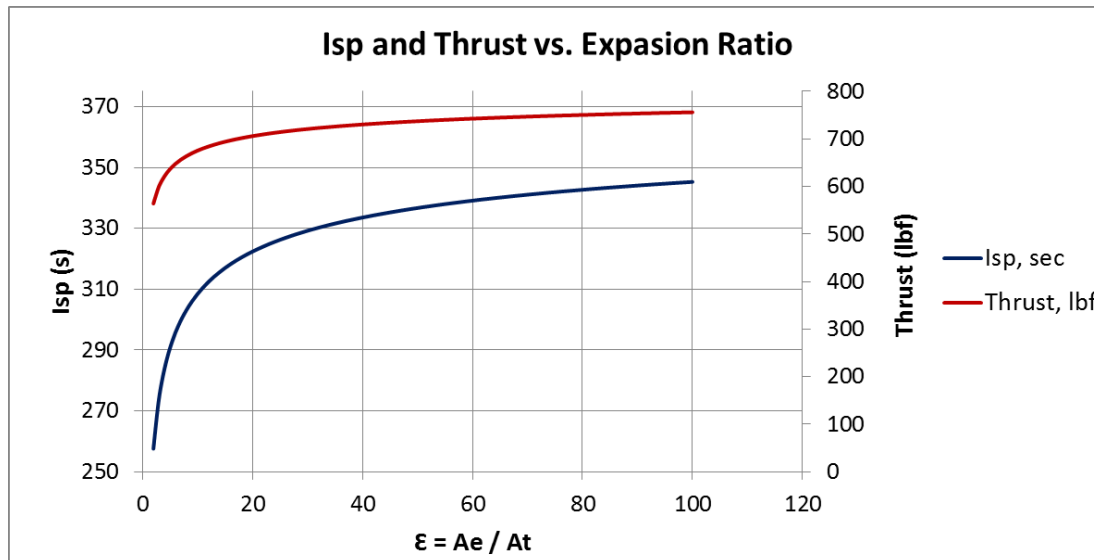


Figure 5.5. Isp and Thrust (vacuum) vs. expansion ratio @ 235 psi chamber pressure

As one can see from the figure 5.5, at about an expansion ratio of 60 the Isp and thrust gain starts to asymptote. An expansion ratio of 30 was chosen due to envelope constraints given by the vehicle but we still get a good increase in thrust and Isp. For ambient testing, the nozzle will have an area expansion ratio of 1.6. Whenever the engine is ready to fly in space, a nozzle extension to 30 will be added.

To determine the design parameters of the bell nozzle, the graphs in figures 5.6 and 5.7 were used as a reference. The design inputs were then put into RPA software to create and output the bell nozzle contour.

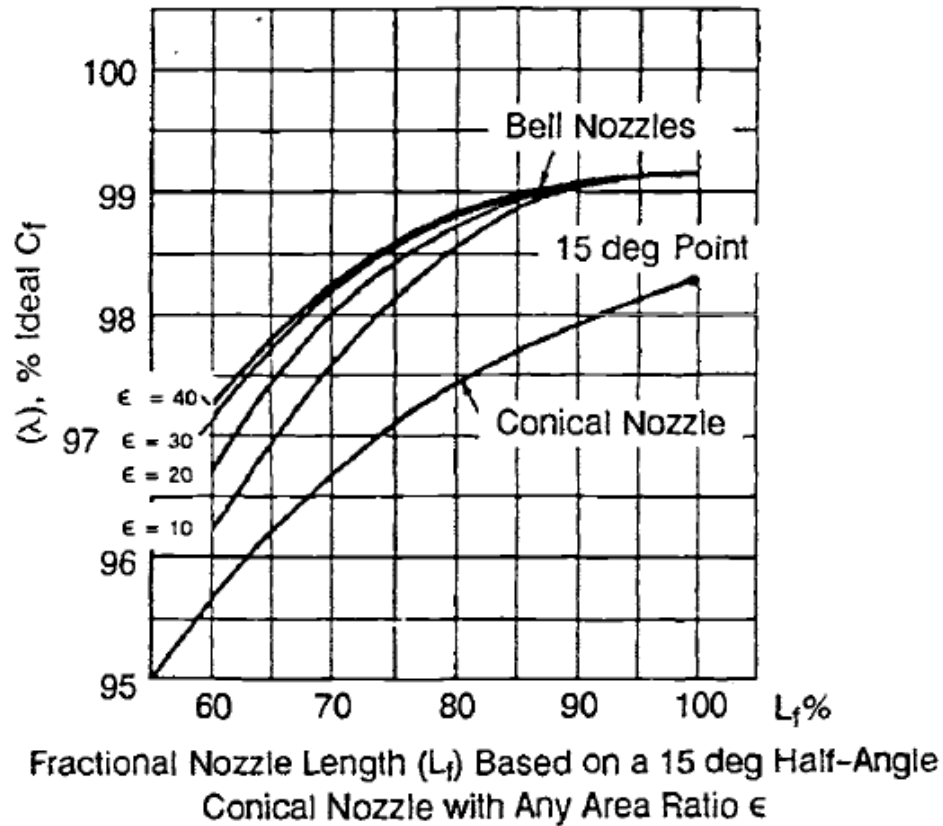


Figure 5.6. Thrust efficiency vs. bell nozzle length (Huzel & Huang, 1992)

A fractional nozzle length ( $L_f$ ) of 80 % was chosen, this means the bell nozzle length is 80% of an equivalent 15 degree half angle conical nozzle. As it can be seen in the figure above, bell nozzles lengths beyond approximately 80% do not significantly contribute to performance, especially when weight penalties are considered<sup>10</sup>.

<sup>10</sup>(Huzel & Huang, 1992)



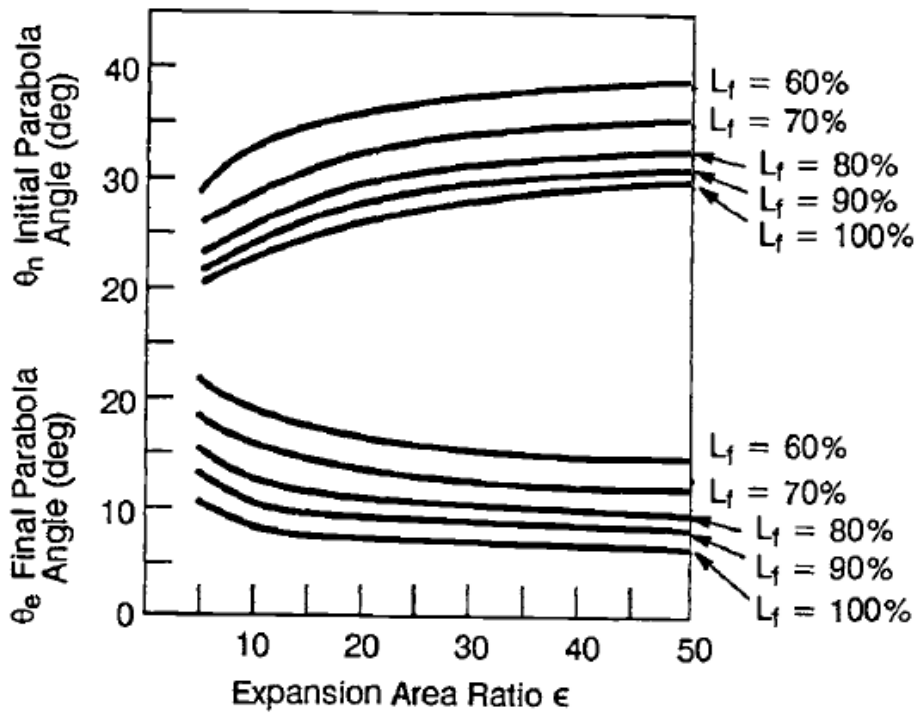


Figure 5.7. Initial and final parabola angle as a function of expansion ratio (Huzel & Huang, 1992)

The initial and final parabola angles were chosen according to the graph above. At a 30 area expansion ratio and 80% fractional nozzle length, the approximate values of initial ( $\theta_n$ ) and final ( $\theta_e$ ) parabola angle are approximately  $30^\circ$  and  $13^\circ$  accordingly. The length of the nozzle was obtained by inputting these parameters into RPA, which came up to 9.87 inches from the throat to the nozzle exit. The final contour of the thrust chamber is shown below in figure 5.8.

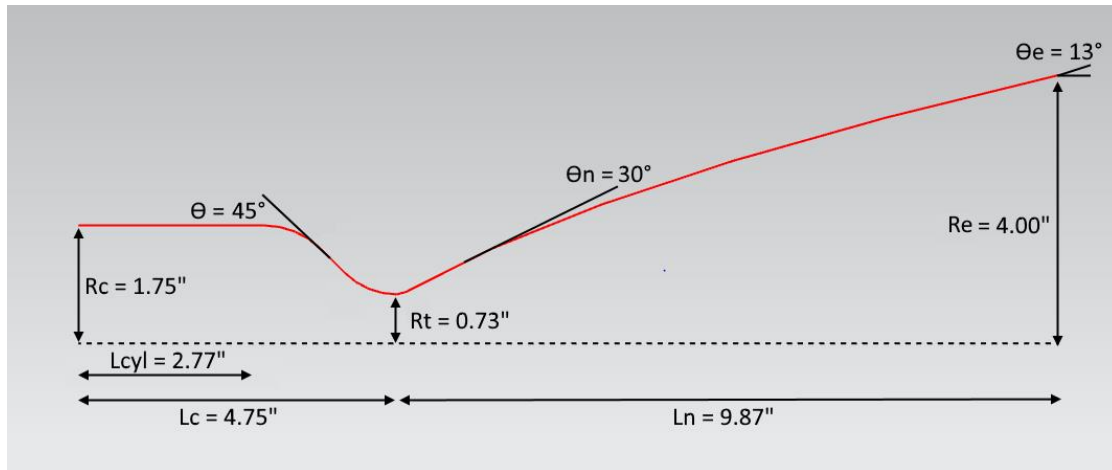


Figure 5.8. CROME thrust chamber final dimensions

## Chapter 6: Injectors Design

The injector is the most critical and complex component of a rocket engine. The injector puts and meters the propellants in the combustion chamber, breaks the propellants into small droplets (a process called atomization), and distributes and mixes the propellants into the appropriate ratio of fuel and oxidizer. The injector design determines the maximum achievable combustion efficiency, the heat transfer rates to the combustion chamber walls, and whether or not low and high frequency combustion instabilities will occur<sup>17</sup>. No other component of a rocket engine has a greater impact upon engine performance. Each percentage point loss in injector combustion efficiency ( $c^*$ ) means a loss of the same magnitude in overall specific impulse ( $I_{sp}$ )<sup>10</sup>.

The choice of injector type, or injection element type, depends on different factors<sup>7</sup>:

- State of the propellants
- Operating conditions such as chamber pressure and mixture ratio
- System pressure drop
- Combustion chamber material and cooling methods used
- Combustion chamber geometry (length and diameter)
- Throttling requirements
- Engine life: restarts and total firing duration

The different and most common injector element types successfully used for liquid-liquid injectors and their advantages and disadvantages are presented in figure 6.1 below.

---

<sup>7</sup>(Gill, Nurick, Keller, & Douglass, 1976)

<sup>10</sup>(Huzel & Huang, 1992)

<sup>17</sup> (Yang, Habiballah, Hulka, & Popp, 2004)

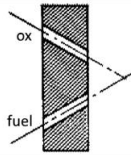
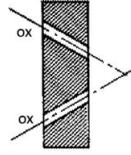
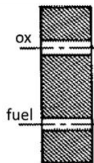
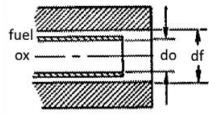
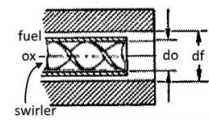
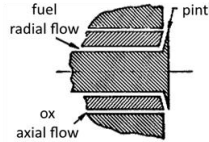
Element Designation	Configuration	Advantages	Disadvantages
Unlike doublet		<ul style="list-style-type: none"> <li>-Proven dependability</li> <li>-Good overall mixing</li> <li>-Simple to manifold</li> <li>-Extensively studied</li> </ul>	<ul style="list-style-type: none"> <li>-Subject to blowpart with hypergolic propellants</li> <li>-Wall compatibility problems due to mixture ratio gradients</li> <li>-Sensitive to design tolerances</li> <li>-Performance sensitive to continuous throttling</li> </ul>
Like doublet		<ul style="list-style-type: none"> <li>-Proven dependability</li> <li>-Good mixing</li> <li>-Very stable element</li> <li>-Not subject to blowpart</li> <li>-Easy to manifold</li> <li>-Excellent for deliberate control of spray for wall compatibility</li> <li>-Extensively studied</li> </ul>	<ul style="list-style-type: none"> <li>-Requires increased axial distance to mix</li> <li>-Sensitive to design tolerances</li> </ul>
Showerhead		<ul style="list-style-type: none"> <li>-Excellent for boundary layer cooling</li> <li>-Excellent for wall compatibility</li> <li>-Easy to manifold</li> <li>-Not subject to blowpart</li> <li>-Proven dependability</li> </ul>	<ul style="list-style-type: none"> <li>-Poor mixing</li> <li>-No definitive characterization</li> </ul>
Shear coaxial		<ul style="list-style-type: none"> <li>-Very good wall compatibility</li> <li>-Low pressure drop</li> </ul>	<ul style="list-style-type: none"> <li>-Poor mixing</li> <li>-Difficult to fabricate if annulus gap is very small</li> <li>-Tends to become unstable when throttled</li> </ul>
Swirl shear coaxial		<ul style="list-style-type: none"> <li>-Good mixing and atomization</li> <li>-Low pressure drop</li> <li>-Proven dependability</li> </ul>	<ul style="list-style-type: none"> <li>-Difficult to fabricate if annulus gap is very small</li> <li>-Tends to become unstable when throttled</li> </ul>
Pintle		<ul style="list-style-type: none"> <li>-Throttleable</li> <li>-Proven dependability</li> <li>-Simple to manufacture</li> <li>-Large thrust per element</li> </ul>	<ul style="list-style-type: none"> <li>-Wall compatibility problems</li> <li>-No correlation for level of mixing and spray size</li> </ul>

Figure 6.1. Common types of liquid-liquid injector elements (Gill, Nurick, Keller, & Douglass, 1976)

The unlike impinging doublets and the pintle type injector were chosen for the engine injector designs. Two different designs were chosen because of their different capabilities, the final decision for the flight vehicle engine will be based on the firing test data for each.

The unlike impinging elements were chosen because they offer good mixing right at the impinging point and the combustion of the propellants occur closer to the injector face. This requires a shorter combustion chamber hence a smaller area to film cool. In contrast, like impinging elements are more stable but require a longer chamber because the mixing and

combustion occurs downstream of the impinging point. Impinging elements (like and unlike) are performance sensitive to continuous throttling but they do not go unstable as much as coaxial elements<sup>7</sup>.

The pintle injector was chosen for two main reasons; first, it is easier for mechanical throttling, and second, it is reported to be highly resistant to combustion instability<sup>6</sup>. The pintle injector is relatively easy to design and manufacture compared to other designs but on the downside, it may result in low combustion efficiency.

## SECTION 6.1: THEORETICAL FLOW ANALYSIS

The flow through the injection elements of an injector can be analyzed using Bernoulli's equation<sup>4</sup>:

$$P_1 + \frac{1}{2}\rho V_1 + \rho g h_1 = P_2 + \frac{1}{2}\rho V_2 + \rho g h_2 + H_L \quad (6.1)$$

it is assumed that  $V_2 \gg V_1$ , therefore  $V_1 \approx 0$ , and there is no potential energy  $h_1 = h_2 = 0$ . The head loss ( $H_L$ ) due to sudden contraction is considered and is equal to:

$$H_L = \frac{h_l V^2}{2g} \quad (6.2)$$

Using the Bernoulli equation with the assumptions described, the head loss equation, and knowing that velocity is equal to  $V = \frac{\dot{m}}{\rho A_{inj}}$ , one can rearrange and calculate the area of injection and orifice diameter:

---

<sup>7</sup>(Gill, Nurick, Keller, & Douglass, 1976)

<sup>6</sup>(Dressler & Bauer, 2000)

<sup>4</sup>(Cimbala & Cengel, 2006)

$$A_{inj} = \dot{m} \sqrt{\frac{2.238 h_l}{\rho \Delta P}}, (in^2) \quad (6.3)$$

$$d = \sqrt{\frac{4 A_{inj}}{N \pi}}, (in) \quad (6.4)$$

where  $\dot{m}$  = flowrate, lb/s ;  $\rho$  = density of propellant, lb/ft<sup>3</sup> ;  $h_l$  = head loss coefficient, 1.7 for a sharp-edged orifice;  $\Delta P$  = pressure drop, psi ; N = number of orifices.

To calculate the injection velocity and pressure drop, one can rearrange the area of injection formula to obtain the following expressions:

$$V = \frac{144}{\rho \sqrt{\frac{2.238 k}{\rho \Delta P}}}, \left(\frac{ft}{s}\right) \quad (6.5)$$

$$\Delta P = \frac{1}{\frac{\rho A_{inj}^2}{2.238 k \dot{m}^2}}, (psi) \quad (6.6)$$

For a throttling engine with fixed areas of injection, it is good practice to design to the minimum of mid-range chamber pressure so that the pressure drop at the low end is high enough, at least 20% of chamber pressure, to prevent low frequency instabilities (also known as Chugging). The resulting areas of injection and injection velocity can then be calculated. As a rule of thumb, the pressure drop has to be at least 20% of the chamber pressure to mitigate low frequency instabilities. The pressure drop and injection velocity at any throttling level (different flow rate) can then be derived from the flow formulas presented above. In the case of a variable injection area injector (i.e. variable pintle injector), one has to design to a minimum area of

injection limited by the manufacturing capabilities and then compute the rest of the flow characteristics using the flow formulas.

For the impinging injector, the design pressure drop at the low end thrust is 14 psi, 20% of the chamber pressure (70 psi). The total area of injection at this pressure drop and the corresponding flow rates for LCH<sub>4</sub> (0.18 lb/s) and LOX (0.48 lb/s) are 0.018 in<sup>2</sup> and 0.030 in<sup>2</sup> accordingly. Having the areas defined, the pressure drop and the injection velocities for the entire thrust range can be calculated. The pressure drop ranges from 14 – 155 psi for both propellants and the injection velocity ranges from 54 – 179 ft/s for LCH<sub>4</sub> and 33 – 109 ft/s for LOX.

The first iteration of the pintle injector is a fixed area design at 500 lbf. The data gathered during testing will be used to design the second iteration which will be a variable area pintle. The design pressure drop for LOX and LCH<sub>4</sub> are 50 and 80 psi at 235 psi P<sub>c</sub> and 500 lbf thrust. The equated areas of injection are 0.052 in<sup>2</sup> for LOX and 0.025 in<sup>2</sup> for LCH<sub>4</sub> for their corresponding flow rates. The derived injection velocity is 62 ft/s for LOX and 128 for LCH<sub>4</sub>.

It was decided to design the first iteration of the pintle injector at 500 lbf to make it less expensive and obtain experience testing the engine. This pintle will to be throttled through the valvesto test and understand the challenges and limits of throttling to use in future injector designs.

For both injectors, the film cooling orifices were designed to a pressure drop of 14 psi and to its low end flow rate of 0.05 lb/s. The area of injection equated to 0.006 in<sup>2</sup> which equals to a hole diameter of 0.02 in.

## **SECTION 6.2: IMPINGING INJECTOR DESIGN**

Impinging jets are the most straightforward way of mixing two different fluids. It consists of two fluid jets colliding at a point (impingement point). The impact produces a fan shaped

spray made up of a mixture of the two fluids. The spray spreads at a resultant angle (beta angle) which is computed from the sum of the combined momentum angles<sup>14</sup>.

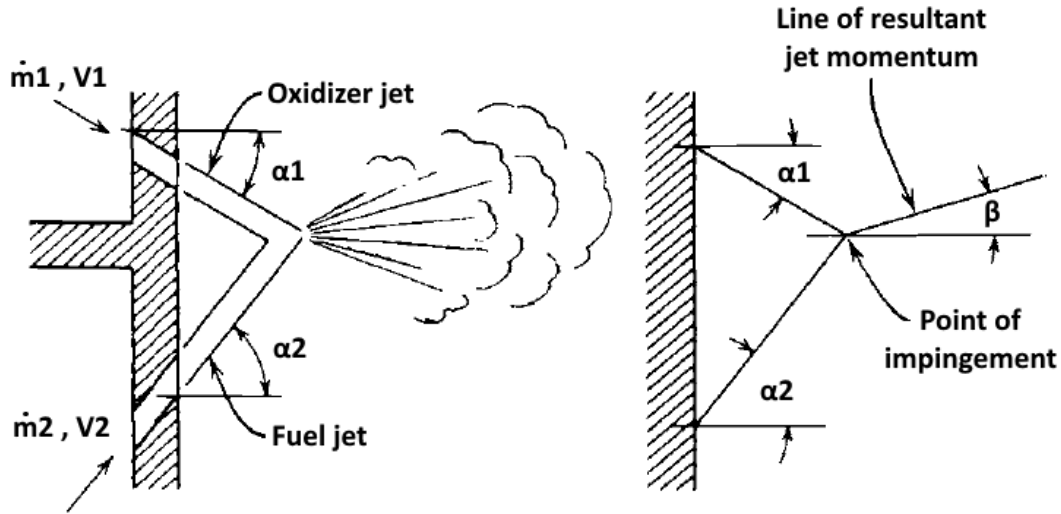


Figure 6.2. Angular relation of doublet impinging streams (Sutton & Biblarz, 2010)

$$\tan \beta = \frac{\dot{m}_1 V_1 \sin \alpha_1 - \dot{m}_2 V_2 \sin \alpha_2}{\dot{m}_1 V_1 \cos \alpha_1 + \dot{m}_2 V_2 \cos \alpha_2} \quad (6.7)$$

### 6.2.1. Injector Face

The CROME engine impinging injector consists of 34 pairs of fuel and oxidizer impinging orifices oriented  $30^\circ$  from the chamber axis ( $\alpha_1$  and  $\alpha_2$ ) and distributed in two concentric rings with 12 pairs in the inner ring and 22 in the outer ring. The total number of orifices was chosen based on manufacturing constraints on orifice diameter, tolerances, and tools availability (standard drill bits).

Eighteen film cooling orifices and eighteen  $\frac{1}{4}$ " acoustic cavities are found on the periphery of the chamber, alternating positions to avoid coolant getting into the cavities and affecting dampening. Nine cooling orifices are at  $25^\circ$  and nine at  $20^\circ$  to reach further down the

<sup>14</sup>(Sutton & Biblarz, 2010)



chamber walls. Finally, a flange bolt pattern of 10 3/8” bolts will serve as the interface between the injector and the chamber. The injector face features described are shown in figure 6.3.

Parameter	Value
# of injection orifices	68 total ; 34 LOX and 34 LCH4
Orifice diameter	0.033” LOX ; 0.026” LCH4
Film cooling orifice diameter	0.020”

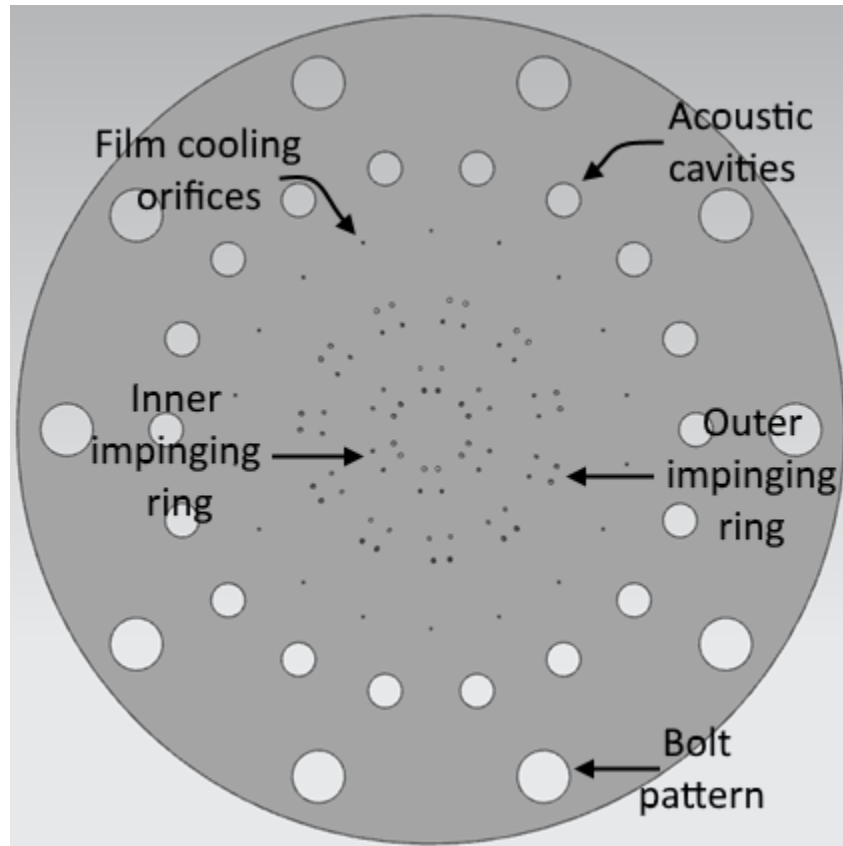


Figure 6.3. CROME impinging injector face configuration

The impingement resultant angle equated to be  $8^\circ$  from the chamber axis. The inner ring was designed to be at  $+8^\circ$  and the outer ring at  $-8^\circ$ . This will avoid directing the propellant mixture towards the chamber wall from the outer ring and it might help with mixing as both fans resultant angles point toward each other. This will give a net momentum angle from both rings of  $0^\circ$  as shown in figure 6.4.

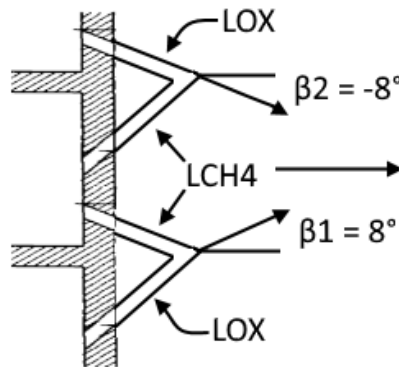


Figure 6.4. Impingement resultant angle for CROME impinging injector

### 6.2.2. Injection Orifices Design Guidelines

The most important parameters to consider when designing impinging elements are length over diameter ratio ( $L/d$ ), impinging angle ( $\alpha$ ), oxidizer to fuel diameter ratio ( $d_o/d_f$ ), and free stream or impingement distance ( $L_{fs}$ ). These parameters have an effect on engine performance and they are mostly determined by testing and previous experience.

Having a large enough  $L/d$  is important to avoid a phenomenon called hydraulic flip, which is the detachment of the jet from the orifice wall which leads to unstable and unpredictable flow. This will affect the alignment of the impinging points causing a fluctuation of mixture ratio. A study done by the Apollo Service Propulsion Systems team showed that orifice  $L/D$  of at

least 4 was required to produce streams concentric with the orifice centerline<sup>7</sup>. The  $L/d$ 's for the injector are 9.6 and 7.6 for LCH<sub>4</sub> and LOX accordingly, and 12.5 for fuel film cooling orifices.

Studies show that for unlike impinging elements, the greater the impinging angle, the greater the quantity of mixed propellant flowing back toward the injector face causing an increase in heat flux<sup>7</sup>. According to NASA's Liquid Rocket Injector document, most unlike-impinging injectors have been designed with impingement angles of 60° ( $\alpha=30^\circ$  from chamber axis).

A study made by JPL (Jet Propulsion Laboratory) on impinging jets found that an oxidizer to fuel orifice diameter ratio ( $d_o/d_f$ ) varying significantly from 1.22 (the study was done to up to 1.5) on unlike impinging jets affects the level of mixing dramatically<sup>7</sup>. The  $d_o/d_f$  for the designed impinging injector is 1.27, which is close to the 1.22 suggested by this study.

For all impinging elements, long free stream or impingement distance ( $L_{fs}$ ) result in the impingement of streams that are partially disintegrated which can cause miss alignment of the jets<sup>7</sup>. This will affect the mixing uniformity of the propellants. A value of the ratio between impingement distance to orifice diameter ( $L_{fs}/d_{orifice}$ ) should be kept between 5 and 7 to minimize stream misimpingement<sup>7</sup>. The  $L_{fs}/d_{orifice}$  values for the CROME impinging injector are 5.2 for LOX and 6.5 for LCH<sub>4</sub>.

### 6.2.3. Manifolds Design

A manifold is the part of the injector that encloses the propellants to feed and distribute it to the injection orifices. The goal of a manifold design is to have the smallest volume (dribble volume) possible, distribute the propellant as evenly as possible across all the injection orifices,

---

<sup>7</sup>(Gill, Nurick, Keller, & Douglass, 1976)

<sup>7</sup>(Gill, Nurick, Keller, & Douglass, 1976)

and be simple to manufacture and assemble. The manifolds design were done after identifying the injection orifice parameters and their layout on the back side of the injector face (inlet). Figures 6.5a, 6.5b, and 6.5c show the orifice layout on the back side of the injector plate, an isometric view of the injector, and a cross section detailing the design of the manifolds. The green color represents LOX and red LCH4.

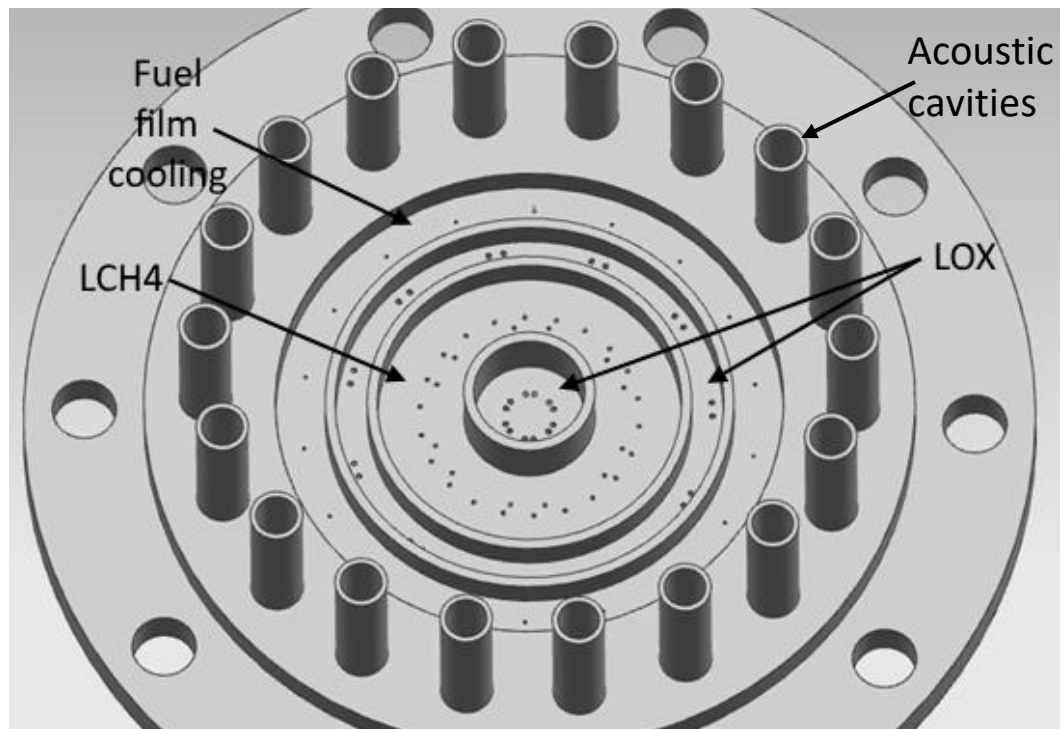


Figure 6.5a. Injector orifice layout at the inlet side

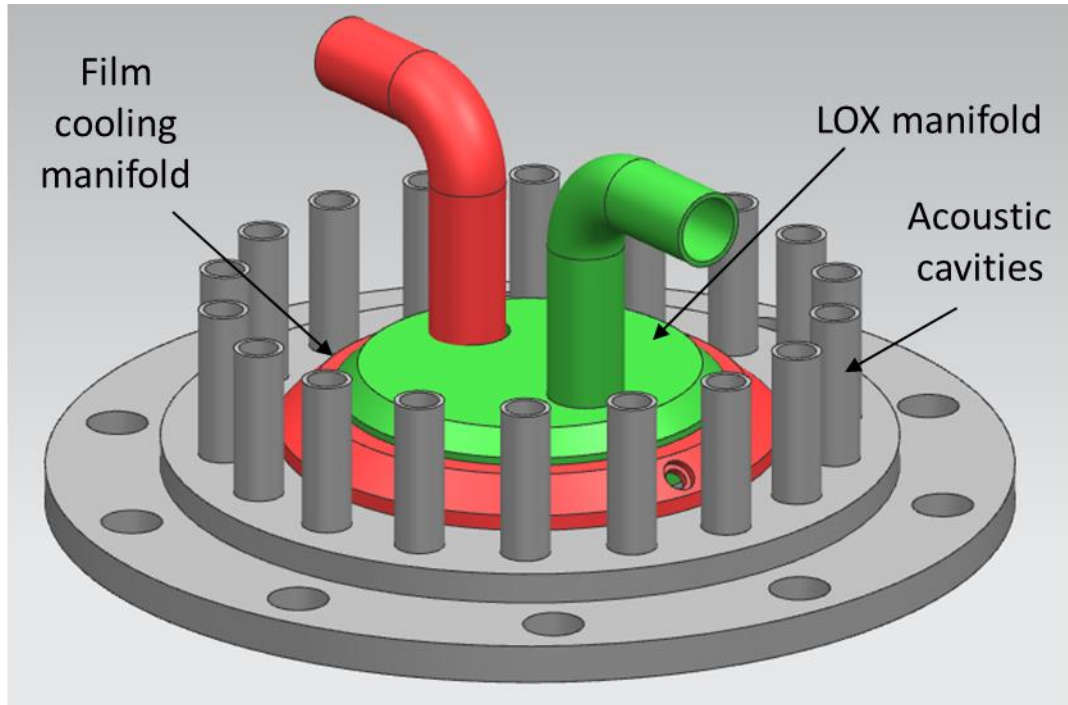


Figure 6.5b. Isometric view of the closure of the manifolds

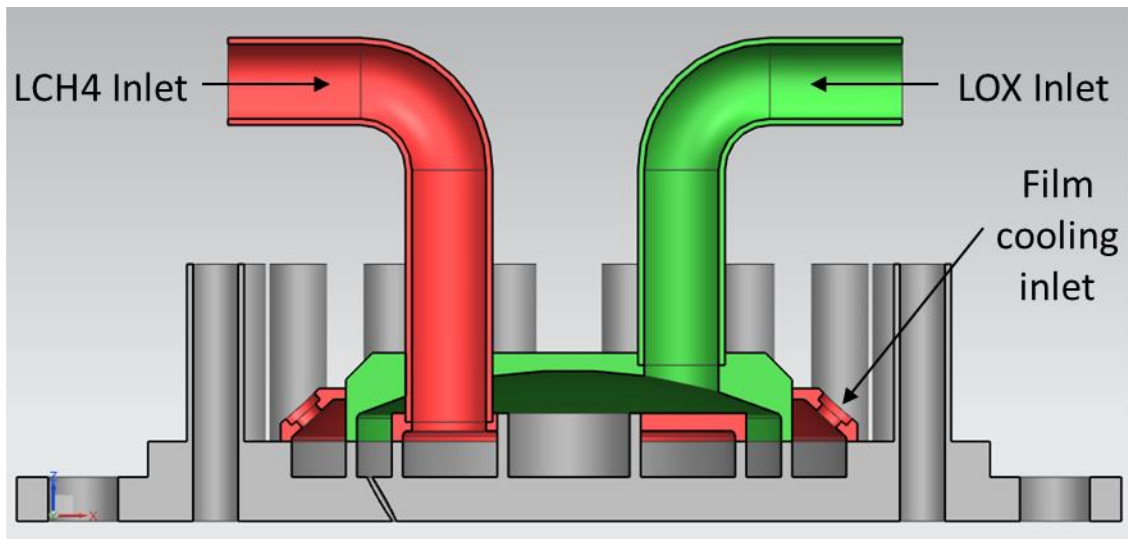


Figure 6.5c. Cross sectional view of impinging injector showing manifold distribution

The LCH<sub>4</sub> and film cooling manifolds are shaped as a ring and the LOX manifold as a dome. The walls are part of the injector plate to avoid welding directly on the surface to prevent

distorting the injection orifices. The inlets for the LCH<sub>4</sub> and LOX are both standard ½” tubes welded to the manifolds. The LOX inlet was placed on top of the LCH<sub>4</sub> manifold to serve as a deflection plate to prevent high static pressure acting on the orifices. This is caused by dumping high pressure and high velocity propellant directly to the orifices. The film cooling has two 3/16” inlets to have a better pressure distribution of the propellant. The film cooling will be fed from the main LCH<sub>4</sub> feed line and a needle valve will be used to test different film cooling percentages only for the first test configuration. Lastly, the ignition system for the engine will be the torch igniter developed by cSETR. Due to space constraints, the igniter will be placed on the combustion chamber.

### **SECTION 6.3: FIXED PINTLE INJECTOR DESIGN**

A pintle injector consists of one of the propellants flowing down the inside of a pintle that has a series of holes or slots close to the tip that injects the propellant radially. The other propellant leaves the manifold through an annular gap creating an axial concentric sheet around the base of the pintle. Mixing and atomization of the propellants result from the collision between the radial jets and the annular sheet. Figures 6.6a-c shows pictures of a water test performed on a single pintle injector. Figure 6.6a shows the flow through the axial or annular injection, 6.6b shows the flow through the pintle or radial flow, and 6.6c show both stream combined<sup>17</sup>.

---

<sup>17</sup>(Yang, Habiballah, Hulka, & Popp, 2004)

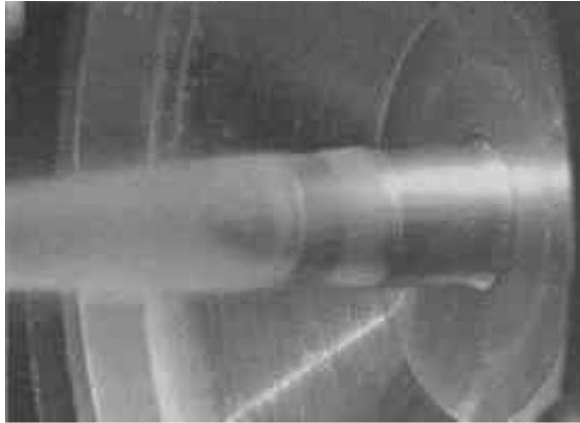


Figure 6.6a. Pintle axial/annular flow(Dressler & Bauer, 2000)



Figure 6.6b. Pintle radial flow(Dressler & Bauer, 2000)

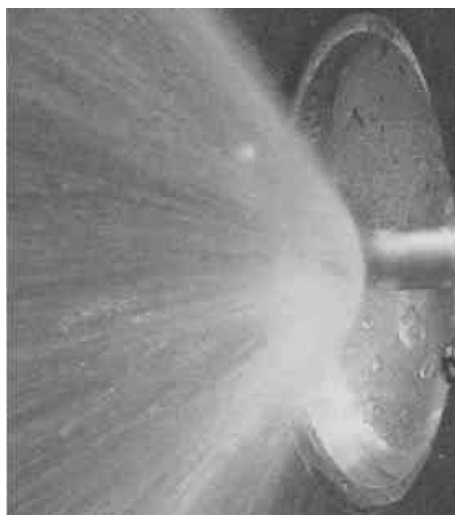


Figure 6.6c. Pintle combined flow- axial and radial(Dressler & Bauer, 2000)

### 6.3.1. Design Guidelines

The colliding of the radial and axial streams creates a fan in the shape of a cone which angle is governed by the ratio of momentums between the radial and the axial streams called the Total Momentum Ratio (TMR):

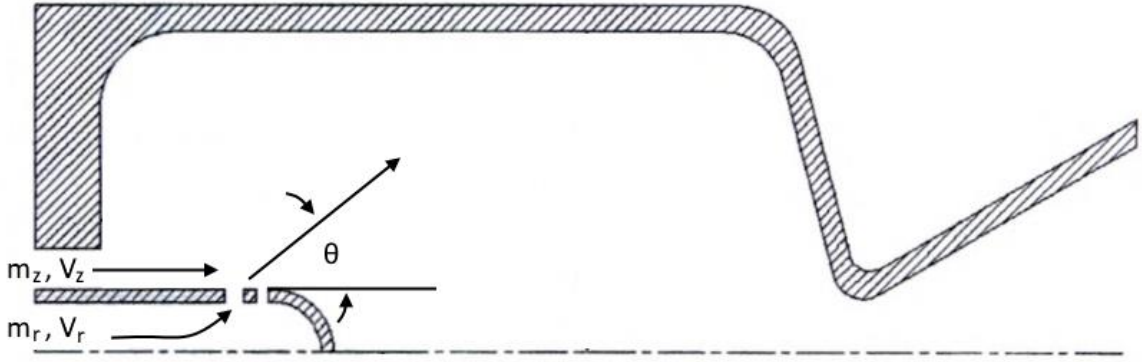


Figure 6.7. Pintle injector streams angular relation

$$TMR = \frac{(\dot{m}V)_r}{(\dot{m}V)_z} \quad (6.8)$$

$$\theta = \arctan(TMR) \quad (6.9)$$

According to Anderson et Al. experience shows that TMR values near unity (or  $\theta=45^\circ$ ) provides optimal performance<sup>17</sup>. The value selected is 0.77 which gives a spray angle of  $40^\circ$ .

The pintle injector is designed as a fuel center pintle; that is LCH<sub>4</sub> as the radial flow and LOX as the annular sheet. This was decided to prevent direct injection of LOX directly to the chamber walls to prevent material compatibility issues. The film cooling will be supplied the same as the impinging injector, through holes on the periphery of the injector plate. The acoustic

---

<sup>17</sup>(Yang, Habiballah, Hulka, & Popp, 2004)



cavities are also configured the same as the impinging injector to be able to use the same thrust chamber.

The skip distance ( $L_s$ ) is the distance the annular flow needs to travel before making contact with the radial flow. A typical value of the skip distance divided by the pintle diameter ( $L_s/D_p$ ) is close to 1. Larger skip distances are subject to substantial deceleration of the annular flow due to friction against the pintle post; whereas short skip distances may lead to spray impingement on the injector face increasing heat flux<sup>17</sup>. The  $L_s/D_p$  chosen for the design is 1, which equals to a  $L_s$  of 3/8" with a pintle diameter of 3/8".

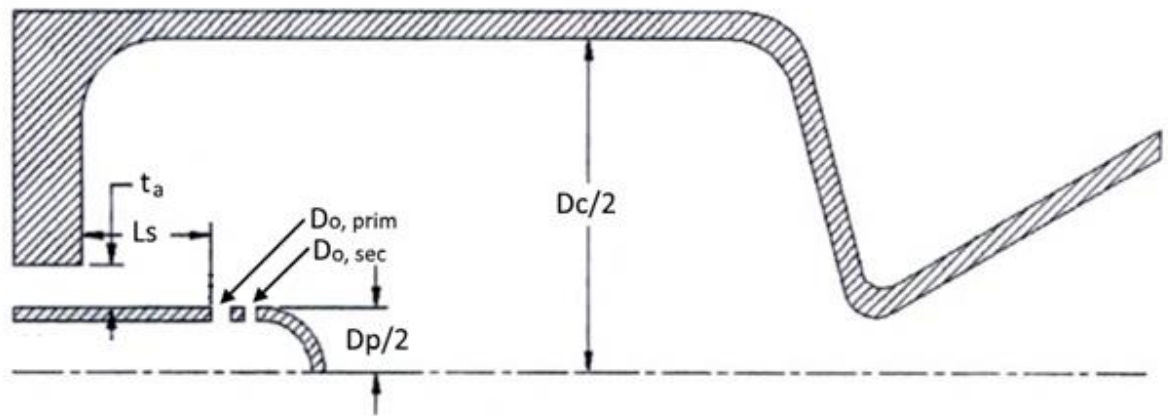


Figure 6.8. Key design variables for a pintle injector

The blockage factor (BF) is defined as the ratio of the total injection holes circumferential length to the pintle circumference. In other words, how much of the pintle circumference the injection orifices cover.

$$BF = \frac{N D_o}{\pi D_p} \quad (6.10)$$

where  $N$  is the number of orifices. A blockage factor of 1 indicates that mixing is caused completely by collision. As the blockage factor decreases, the mixing is less by collision and more by shear. TRW's experience has been with blockage factors between 0.3 and 0.7<sup>15</sup>. To improve mixing, some designs implement a secondary set of holes placed downstream of the primary holes. They are placed circumferentially to cover the gaps left by the primary holes<sup>17</sup>.

For the CROME pintle, the size and number of holes on the pintle post was limited by manufacturing capabilities and tooling. A secondary set of holes was added to improve mixing. There are 9 primary holes with a diameter of 0.04" and 9 secondary holes of 0.031". The blockage factor computed to be 0.54 with a pintle diameter of 3/8". The annulus thickness ( $t_a$ ) is 0.028" with a tolerance of  $\pm 0.001$ ".

### **6.3.2. Manifolds Design**

The manifolds for the pintle injector are very straightforward. The pintle post is fed directly through a 3/8" tube and the LOX manifold is a dome type fed through a 1/2" tube. The film cooling manifold is a ring type with two 1/4" inlets that feed through the main LCH4 feed line and its flow will be controlled by a needle valve to test different cooling percentages. The cSETR igniter will be placed on the face of the pintle injector through a 3/8" tube and a special adapter to fit its size.

A special feature is to use an interchangeable pintle to be able to replace it if damaged or to test different configurations and designs. To achieve this, the pintle post has a flange that fastens through 8-32 studs and nuts to the LOX manifold and will be sealed using a Gore seal. One of the major challenges faced with the design is the alignment of the pintle post and the high tolerances needed for the annular gap. To help with this, three fins were added to the annular gap

---

<sup>15</sup>(Woodward, Miller, Bazarov, Guerin, Pal, & Santoro, 1998)

to keep the pintle centered and aligned. Figures 6.9a-c show an isometric view of the pintle injector and a cross section of the design.

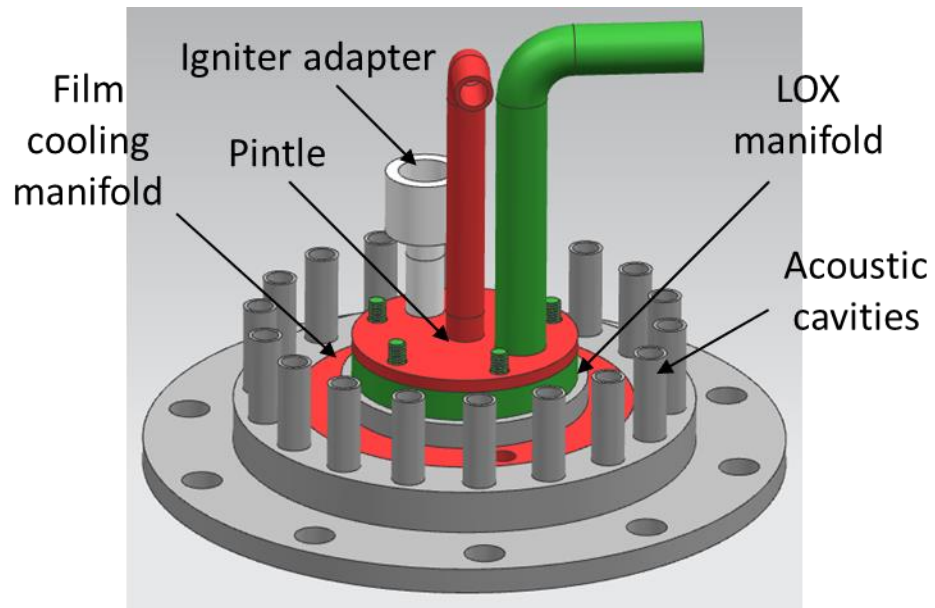


Figure 6.9a. Isometric view of pintle injector

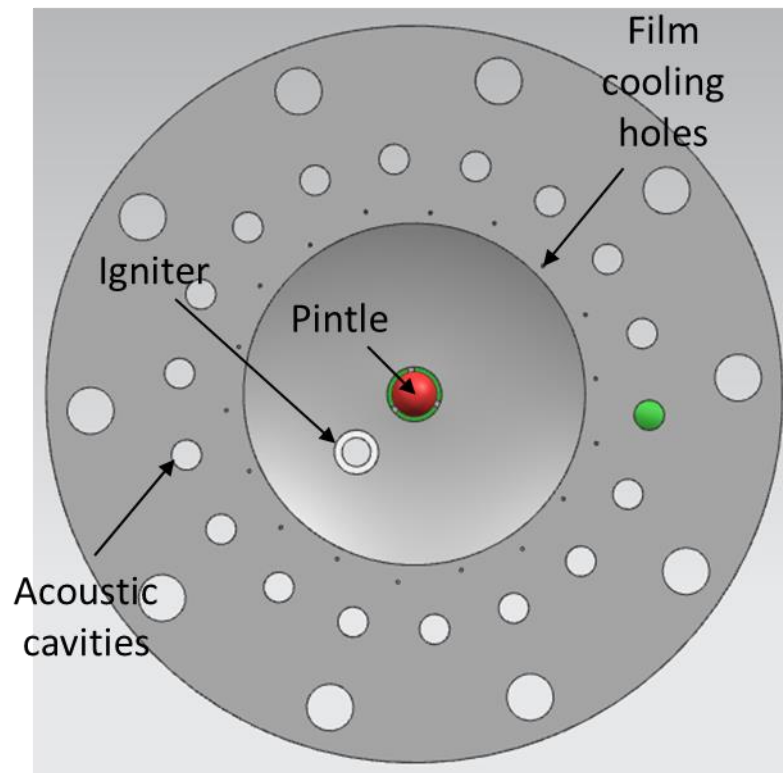


Figure 6.9b. Pintle injector face configuration

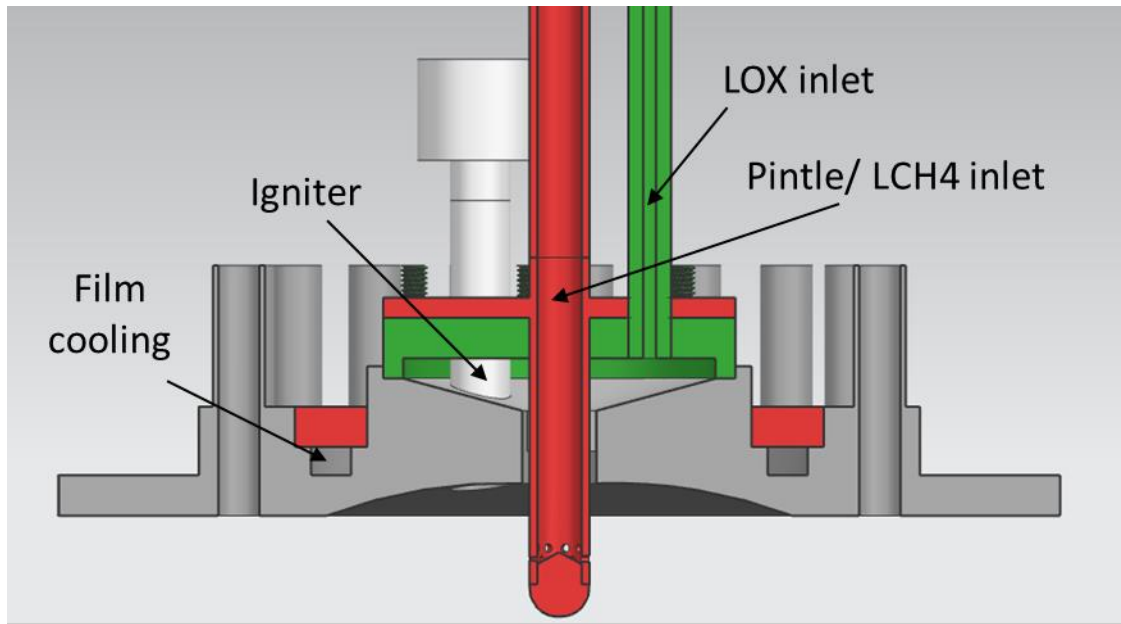


Figure 6.9c. Cross section view of pintle injector showing manifold distribution

A second version of the pintle injector was developed for testing purposes. This version was designed with interchangeable or non-welded parts. This design allows for the easy access and modification of different feature to find the optimal parameters for the final flight version. Figure 6.10a and 6.10b shows and isometric and cross sectional view of this second version.

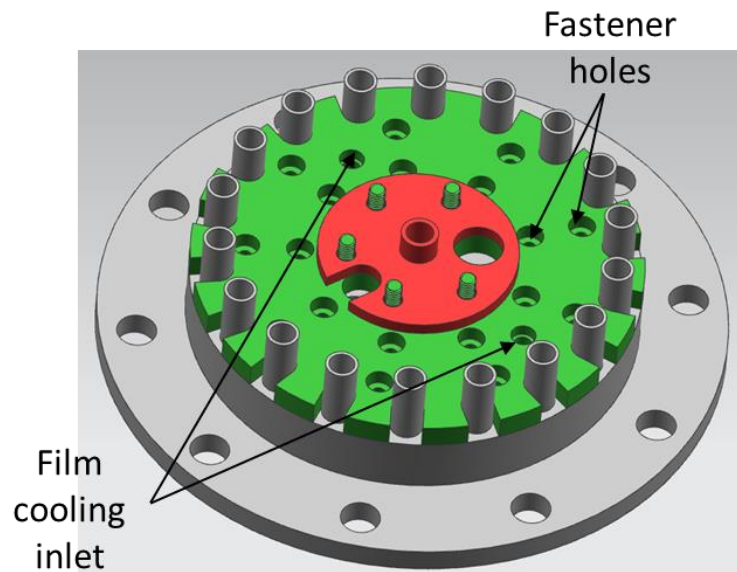


Figure 6.10a. Isometric view of non-welded version of pintle injector

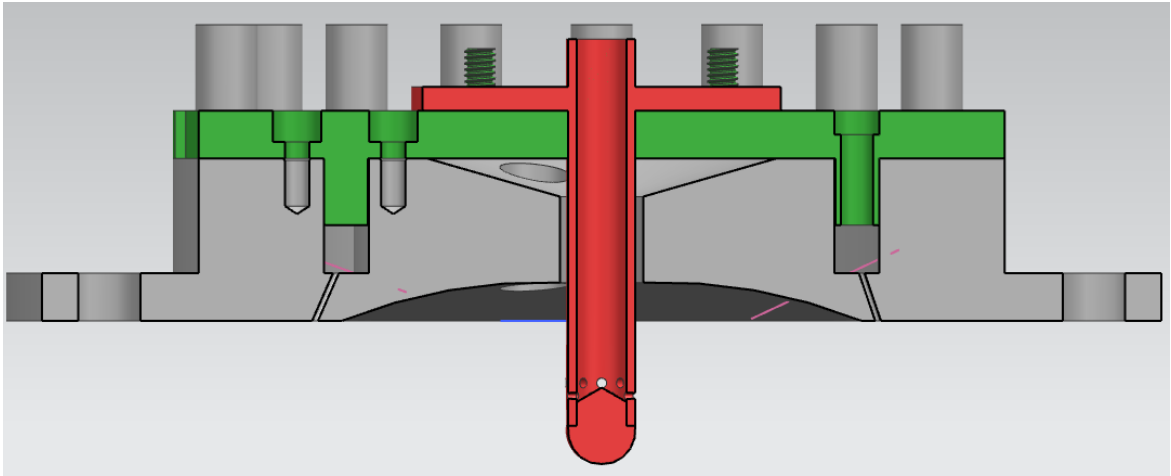


Figure 6.10b. Cross section view of non-welded version of pintle injector

## SECTION 6.4: COMBUSTION INSTABILITY ANALYSIS

### 6.4.1. Introduction to Combustion Instabilities

Combustion instability problems have always been present during nearly every rocket engine development program. Combustion instabilities severely impair the operation of the engine; they can cause high pressure vibration forces and high heat transfer that can lead to catastrophic failure. In general, combustion instability is caused by the coupling of the combustion process and the fluid dynamics of the engine system. By this coupling, the combustion process delivers energy to pressure and velocity oscillations in the combustion chamber increasing heat transfer and causing the melting of the injector and chamber<sup>5</sup>.

There are three types of combustion instabilities in liquid rocket engine: low, medium, and high frequency instabilities. Low frequency instabilities (10-400 Hz), also known as chugging, are caused by the pressure interaction between the combustion chamber and

---

<sup>5</sup>(Douglass, Combs, & Keller, 1975)

the propellant feed system. It will affect engine performance and can introduce high frequency instabilities. Medium frequency instabilities (400-1000 Hz), also known as buzzing, are mostly caused by the stronger coupling between the combustion process and the flow in some part of the propellant feed system. They seldom represent pressure perturbation greater than 5% of the mean combustion chamber and usually are not accompanied by large vibratory energy. They are mostly noisy than destructive, but can induce high frequency instabilities. High frequency instabilities ( $>1000$  Hz), known as screeching or screaming, are the most dangerous and destructive and can destroy an engine in less than 1 second. They are linked to the combustion process forces (pressure waves) and chamber acoustical resonance properties<sup>14</sup>.

To mitigate low and medium frequency instabilities, the injectors' pressure drop is designed to be  $\geq 20\%$  the chamber pressure across all throttle levels. Therefore, this section will focus on high frequency instability and the design of dampening devices.

High frequency instability may occur in two modes, longitudinal and transverse. The longitudinal mode, also called organ pipe mode, acts along axial planes of the combustion chamber. In a rocket engine, the converging section of the chamber produces the main damping of longitudinal modes oscillations; the reflection of waves from the convergent section entrance departs from that of an ideal close end<sup>14</sup>.

The transverse modes propagate along planes perpendicular to the chamber axis and can be broken down in tangential and radial modes. Couple modes combining any of these can also occur. A representation of the three modes of instability is shown in figure 6.11.

---

<sup>14</sup>(Sutton & Biblarz, 2010)

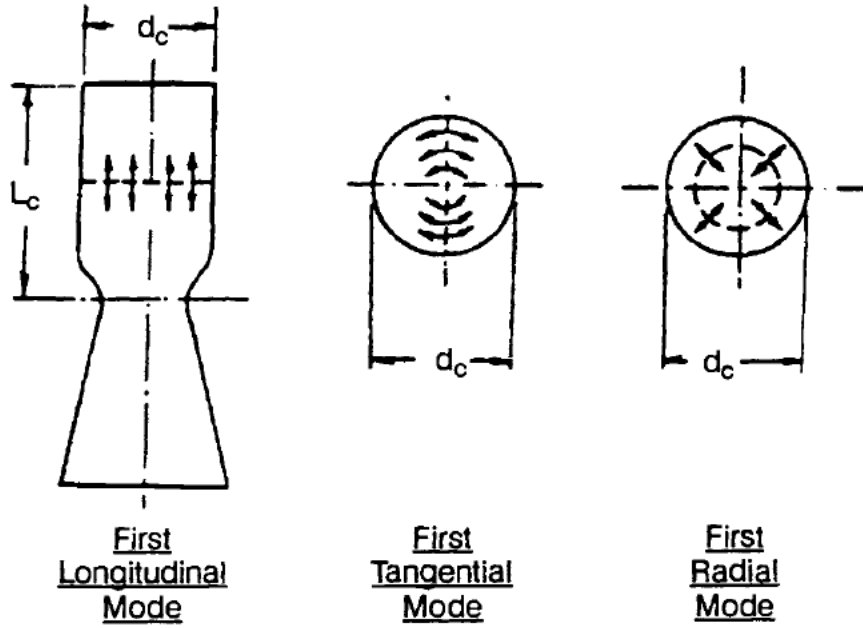


Figure 6.11.High frequency modes of combustion instability(Huzel & Huang, 1992)

#### 6.4.2. High Frequency Instability Analysis

To estimate the resonant frequency at which each mode will occur, the following expression is used as it has showed good theoretical versus experimental agreement<sup>16</sup>.

$$f_{m,n,q} = \frac{c}{2\pi} \sqrt{\left(\frac{\lambda_{mn}}{R_c}\right)^2 + \left(\frac{q\pi}{L_c}\right)^2}, \quad (Hz) \quad (6.11)$$

where  $c$  = speed of sound, ft/s;  $\lambda$  = transversal eigenvalues for mode tangential and radial mode numbers  $m, n = 0, 1, 2, \dots$  from table 6.1;  $q$  = longitudinal mode number  $q = 0, 1, 2, \dots$ ;  $R_c$  = combustion chamber diameter, ft;  $L_c$  = effective acoustic length (chamber length from the face of the injector to the nozzle throat minus half the length of the converging nozzle), ft.

The speed of sound for any gas is computed using the following formula:

$$c = \sqrt{\frac{kRT_c g}{M}} \quad (6.12)$$

<sup>16</sup>(Yang & Anderson, 1995)

where  $k$ = specific heat constant of the combustion gases,(1.143);  $R$ = universal gas constant, ( $1545.35 \frac{ft \cdot lb}{lbmol \cdot R}$ );  $g$ = gravitational constant, ( $32.174 \text{ ft/s}^2$ );  $T_c$ =combustion temperature ,  $R$ ;  
 $M$ =molecular mass of combustion gases,(obtained from RPA = 19.1lb/mol).

Table 6.1. Transversal modes eigenvalues (Yang & Anderson, 1995)

Mode	m	n	$\lambda_{mn}$
1T	1	0	1.8412
2T	2	0	3.0542
1R	0	1	3.8317
2R	0	2	7.0156
1T1R	1	1	5.3314
1T2R	1	2	8.5363

For the speed of sound analysis, RPA was used to estimate the combustion temperature at a mixture ratio of 2.7. The chamber wall temperature profile was plotted assuming only radiation heat transfer through the walls of the chamber and assuming these values as the combustion temperature.

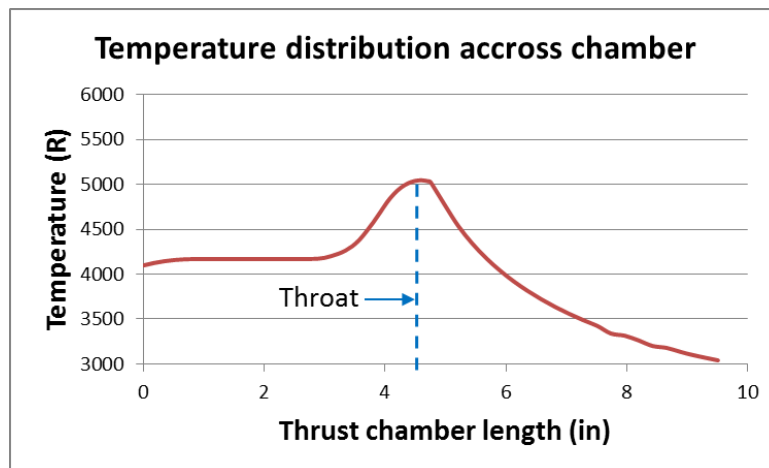


Figure 6.12. Chamber wall temperature distribution across thrust chamber



According to the graph, the assumed combustion temperature ( $T_c$ ) is 4230 R which yields a speed of sound of approximately 3548 ft/s. Using this speed of sound, the eigenvalues shown in table 6.1 for each mode, and the geometric characteristics of the chamber, the estimated resonant frequencies for different modes were calculated and are shown in table 6.2

Table 6.2. Estimated resonant frequencies for the CROME engine

Acoustic Modes	Calculated Resonant Frequency (Hz)
1L	5661.8
1T	7129.5
1T1L	9104.2
2L	11323.7
2T	11826.4
2T1L	13111.9
1R	14837.1
1R1L	15880.7
3L	16985.5
1T1R	20644.2
2R	27165.7
2R1L	27749.5
1T2R	33054.3

Note that not all possible acoustic modes were analyzed; the ones selected were based on the modes analyzed by the NASA JSC Morpheus instability paper<sup>12</sup>.

### 6.4.3. Acoustic Dampening Devices

To dampen or dissipate high frequency acoustic instabilities in a combustion chamber, several methods have been employed. Baffles protruding into the combustion chamber from the injector face have been used successfully to prevent transverse acoustic modes, but they have

---

<sup>12</sup>(Melcher & Morehead, 2014)

little to no effect on longitudinal acoustic modes<sup>5</sup>. Because they are protruding into the combustion chamber, they require having some kind of cooling.

Acoustic absorbers, such as Hemholtz resonators and quarter-wave tubes, are also used to remove oscillatory energy from the system (dampening). They are generally an array of acoustic resonators distributed along the walls of the combustion chamber. Hemholtz resonators consist of small passages connecting the combustion chamber to the resonator cavity. A quarter-wave resonator is a closed slot or tube (usually straight) with a uniform cross sectional area<sup>5</sup>. They are usually placed along the injector periphery or near the injector face to dampen acoustic instabilities where the combustion begins.

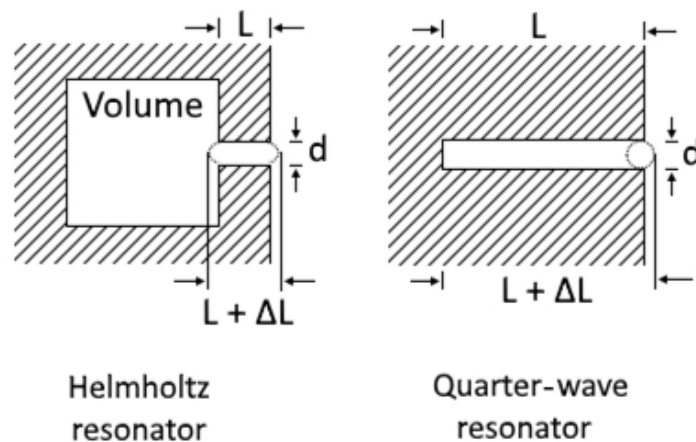


Figure 6.13. Helmholtz and quarter-wave resonators geometric characteristics

Quarter-wave resonators were chosen for the CROME engine because of their simplicity to integrate in the design and they can be made “tunable” by adding a screw to vary the acting length or by replacing the tube. The 1T, 1T1L, 2L, 2T, 2T1L, and 1R modes were determined to be the most critical during a discussion with the NASA Morpheus JSC team. These six

<sup>5</sup>(Douglass, Combs, & Keller, 1975)

frequencies will be the basis for the resonators with a frequency bandwidth of  $\pm 200$  Hz for each, which equals 18 total quarter-wave tubes.

#### 6.4.4. Quarter-wave Resonators Analysis

The design concept of a quarter-wave resonator consists of tuning its frequency ( $f_{qw}$ ) to the frequency of the combustion chamber ( $f_{m,n,q}$ ). The frequency of a quarter-wave cavity is changed by adjusting its length  $L$  according to the following expression:

$$f_{qw} = \frac{c}{4(L+\Delta L)}, \text{ (Hz)} \quad (6.13)$$

where  $c$  is the speed of sound calculated earlier and  $L + \Delta L$  is the length of the cavity plus a correction factor to account for the mass accelerated by the acoustic field outside the resonator, which can be estimated by  $\Delta L = 0.3d$ , where  $d$  is the cavity diameter. The resultant lengths of each of the 18 quarter-wave tubes are presented in table 6.3.

Table 6.3. Lengths of quarter-wave resonators for the CROME engine

Acoustic Mode	Frequencies (Hz)	L (in.)
1T - 200 Hz	6929	1.46
1T	7129	1.42
1T + 200 Hz	7329	1.38
1T1L - 200 Hz	8221	1.12
1T1L	8421	1.09
1T1L + 200 Hz	8621	1.07
2L - 200 Hz	8764	0.88
2L	8964	0.87
2L + 200 Hz	9164	0.85
2T - 200 Hz	11626	0.84
2T	11826	0.83
2T + 200 Hz	12026	0.81
2T1L - 200 Hz	12447	0.75
2T1L	12647	0.74
2T1L + 200 Hz	12847	0.73

1R - 200 Hz	14637	0.65
1R	14837	0.64
1R + 200 Hz	15037	0.63

The length of the quarter-wave tubes are calculated assuming a steady state combustion temperature. At start up, the combustion will start at much lower temperatures and the resonant frequencies of the chamber will be lower. If the temperature is higher of that assumed, the frequencies increase. Doing the analysis at different temperatures, the frequencies change significantly but the length of the quarter-wave tubes are less sensitive and the change is in the ten thousands of an inch. The design feature of having screws to adjust the acting length of the quarter-wave tubes will allow us to fine tune the cavities during testing.

## **SECTION 6.5: ENGINE CONFIGURATION**

The engine configuration was put together to understand how all the components and instrumentation fit in the design envelope to make the necessary design changes before manufacturing the engine. This step helps plan the assembly of the whole engine and prevent design errors. The model includes the structural interface to the vehicle, valves and their structural supports, plumbing, fittings, instrumentation equipment, etc. The following figures show different angles of the engine configuration with parts labeled for reference.

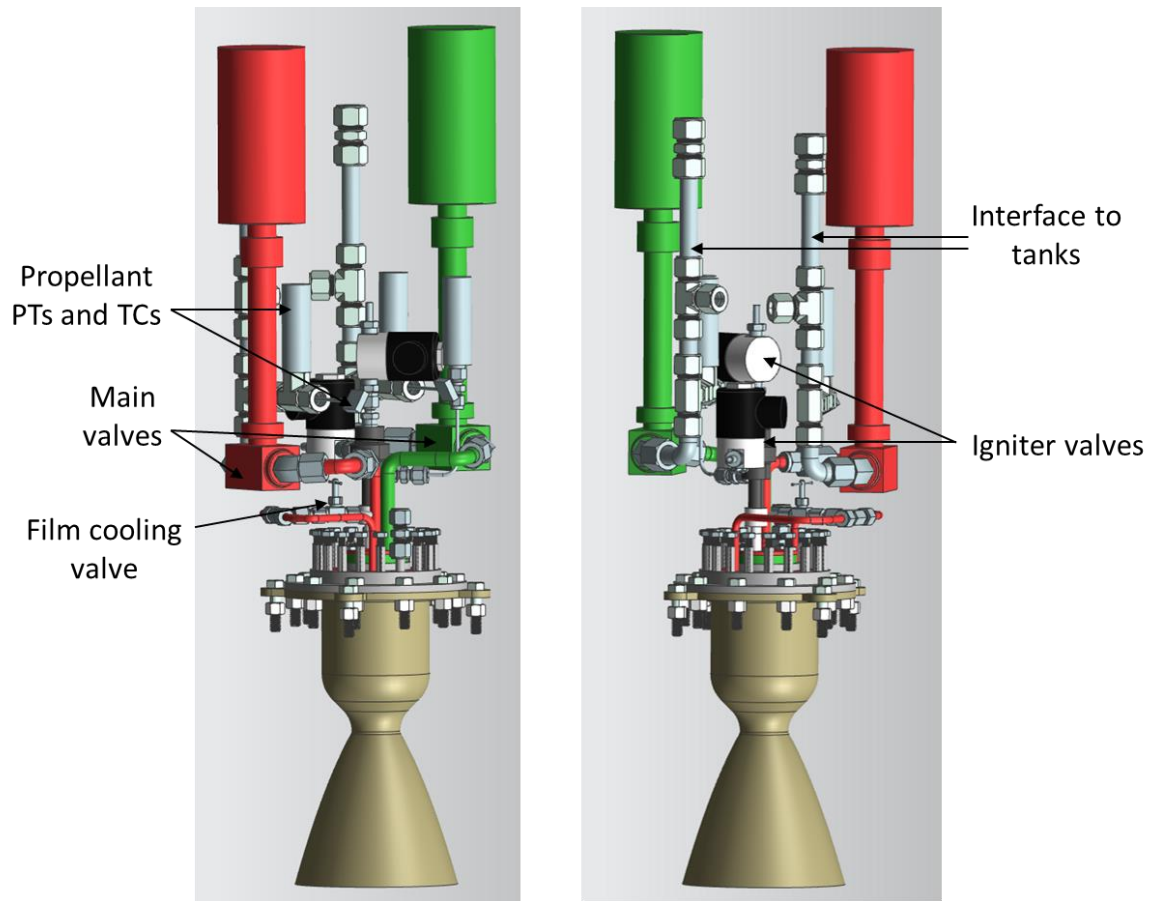


Figure 6.14. Engine infrastructure – propulsion components

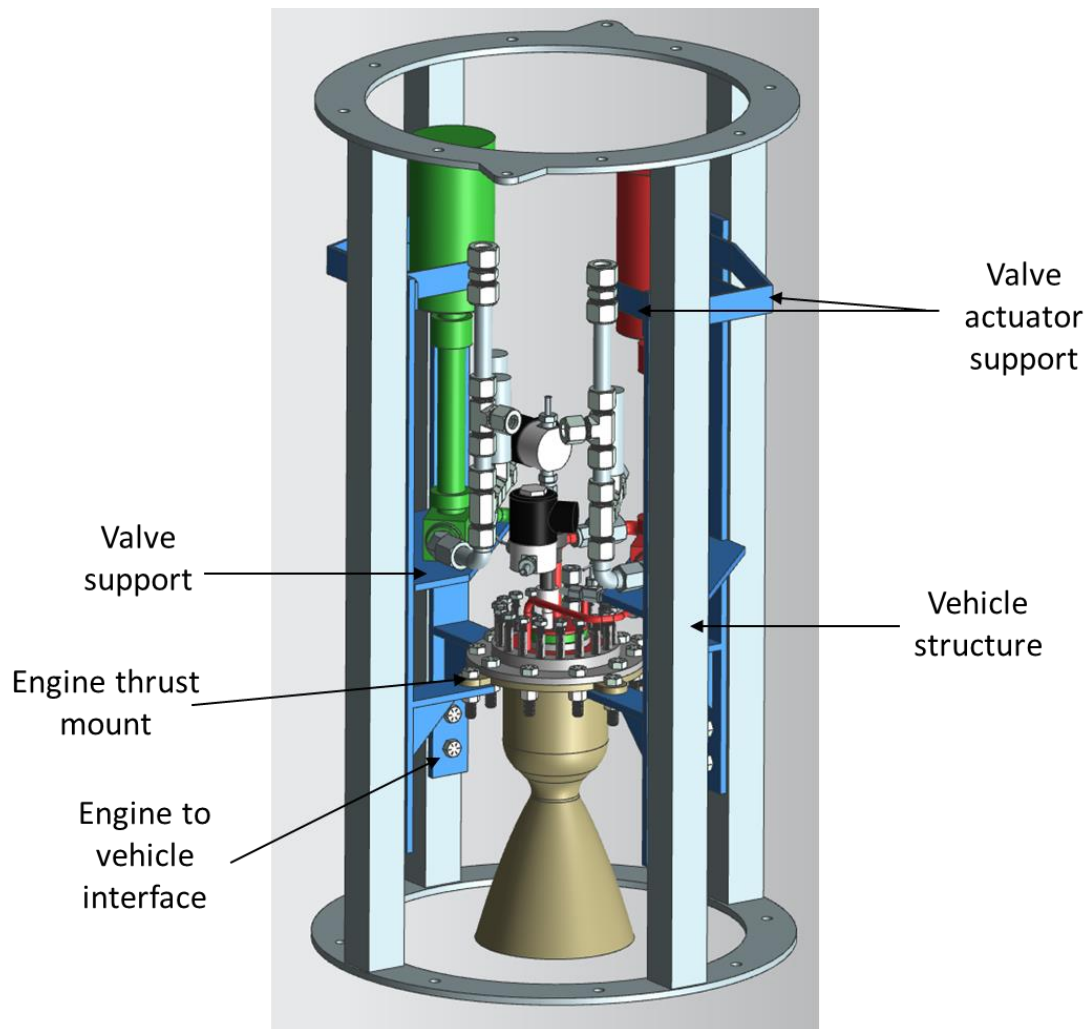


Figure 6.15. Engine infrastructure – structural supports

## Chapter 7: Conclusion and Future Work

The CROME engine was designed by cSETR students in partnership with the National Aeronautics and Space Administration (NASA) to serve as the main propulsion system for Daedalus suborbital vehicle. The purpose of Daedalus mission and the engine is to fire in space under microgravity conditions to demonstrate the performance of an integrated LOX/LCH<sub>4</sub> system in space. There is very limited data concerning LOX/LCH<sub>4</sub> rocket engines fired in space<sup>11</sup> and it is of great interest to assess the CROME engine's performance, restartability, and throttle capabilities under this condition.

The design criteria, theory, and procedures used to design the CROME engine were detailed to aid the future team members working with the design, understand the development process and the reasoning behind the major decisions that formed this engine.

The future work of this project will focus on hot firing test of the engine and getting it ready for space flight. The short to medium term goals for the project are:

- 1- Perform structural, thermal, and flow analysis on thrust chamber and injectors.
- 2- Create manufacturing drawings and fabricate engines using both conventional practices and additive manufacturing.
- 3- Water test of the injectors to validate the design calculations by measuring pressure drop and flow rates. Allow comparison of both the conventional and additive manufactured injectors and to visually assess the atomization of the injection streams and film cooling.
- 4- Procure propulsion components such as the main throttling valves and actuators, as well as instrumentation such as flow meters, pressure transducers, and thermocouples.

---

<sup>11</sup>(Klen)

- 5- Assemble engine and perform hot fire tests at the UTEP Technology Research and Innovation Acceleration Park (tRIAC) located in Fabens, TX.



## Bibliography

- [1]*Inconel Alloy 625*. (2007). Retrieved November 1, 2016, from Special Materials:  
<http://www.specialmetals.com/assets/documents/alloys/inconel/inconel-alloy-625.pdf>
- [2]NASA Sounding Rockets User Handbook. (2015). Wallops, VA: NASA Goddard Space Flight Center.
- [3]Brown, C. D. (1996). *Spacecraft Propulsion*. Washington, D.C: American Institute of Aeronautics and Astronautics.
- [4]Cimbala, J. M., & Cengel, Y. A. (2006). *Fluid Mechanics Fundamentals and Applications*. New York, NY: McGraw-Hill.
- [5]Douglass, H. W., Combs, L. P., & Keller, R. B. (1975). *Liquid Rocket Engine Combustion Stabilization Devices*. Washington, D.C: National Aeronautics and Space Administration.
- [6]Dressler, G. A., & Bauer, J. (2000). TRW Pintle Engine Heritage and Performance Characteristics. *36th AIAA/ASME/SAE/ASEE Joint Propulsion Conference and Exhibit*.
- [7]Gill, G. S., Nurick, W. H., Keller, R. B., & Douglass, H. W. (1976). *Liquid Rocket Engine Injectors*. Cleveland, OH: National Aeronautics and Space Administration.
- [8]Harrje, D. T., & Reardon, F. H. (1972). *Liquid Propellant Rocket Combustion Instability*. Washington, D.C: National Aeronautics and Space Administration.
- [9]Hill, P. G., & Peterson, C. R. (1965). *Mechanics and Thermodynamics of Propulsion*. Reading, MA: Addison-Wesley Pub.
- [10]Huzel, D. K., & Huang, D. H. (1992). *Modern Engineering for Design of Liquid-Propellant Rocket Engines*. Washington, D.C: American Institute of Aeronautics and Astronautics.
- [11]Klen, M. D. (n.d.). *Liquid Oxygen/Liquid Methane Propulsion and Cryogenic Advanced Development*. Cleveland, OH: NASA Glenn Research Center.

- [12]Melcher, J. C., & Morehead, R. L. (2014). Combustion Stability Characteristics of the Project Morpheus Liquid Oxygen/Liquid Methane Main Engine. *50th AIAA/ASME/SAE/ASEE Joint Propulsion Conference and Exhibit*.
- [13]Ponomarenko, A. (2015). *Rocket Propulsion Analysis (RPA)*. Retrieved November 1, 2016, from <http://propulsion-analysis.com/index.htm>
- [14]Sutton, G. P., & Biblarz, O. (2010). *Rocket Propulsion Elements*. Hoboken, NJ: John Wiley & Sons.
- [15]Woodward, R. D., Miller, K. L., Bazarov, V. G., Guerin, G. F., Pal, S., & Santoro, R. J. (1998). Injector Research for Shuttle OMS Upgrade Using LOX/Ethanol Propellants. *34th AIAA/ASME/SAE/ASEE Joint Propulsion Conference and Exhibit*.
- [16]Yang, V., & Anderson, W. E. (1995). *Liquid Rocket Engine Combustion Instability*. Washington, D.C: American Institute of Aeronautics and Astronautics.
- [17]Yang, V., Habiballah, M., Hulka, J., & Popp, M. (2004). *Liquid Rocket Thrust Chambers: Aspects of Modeling, Analysis, and Design*. Reston, VA: American Institute of Aeronautics and Astronautics.

## **Vita**

Jesus Eduardo Trillo attained his Bachelor of Science degree in Mechanical Engineering from the University of Texas at El Paso in the fall of 2014. During his undergraduate studies, he completed an internship at General Motors Co. as a manufacturing engineering intern, one at NASA Marshall Space Flight Center at the propulsion components branch, another at NASA Stennis Space Center at the office of the chief engineer, and one at NASA Johnson Space Center at the energy and propulsion division working on fuel cell technology.

After his undergraduate studies, he pursued his Masters of Science in Mechanical Engineering continuing his research on LOX/LCH<sub>4</sub> rocket engine systems technologies. During his Master's degree, he was selected as a Pathway Intern at NASA Kennedy Space Center to work with the Environmental and Life Support Systems branch developing ground support equipment for SLS rocket and the Orion spacecraft. Jesus E. Trillo accepted a job offer to work at NASA Kennedy Space Center after completing his Master's degree in the fall of 2016.

Contact Information: [trilloje21@gmail.com](mailto:trilloje21@gmail.com)

This thesis was typed by Jesus E. Trillo